Chinese Chemical Letters 37 (2026) 112155

Contents lists available at ScienceDirect

Chinese Chemical Letters

journal homepage: www.elsevier.com/locate/cclet

Synthesis of multi-substituted 9,9′-spirobifluorenes and their applications in organic light-emitting diodes

Zhanhui He[a], Zheng Liu[a,*], Hongji Li[a], Lijun Yang[a], Guodong Yin[a,*], Jingbo Lan[b,*]

[a] Hubei Key Laboratory of Pollutant Analysis and Reuse Technology, College of Chemistry and Chemical Engineering, Hubei Normal University, Huangshi 435002, China

[b] Key Laboratory of Green Chemistry and Technology of Ministry of Education, College of Chemistry, Sichuan University, Chengdu 610064, China

ARTICLE INFO

Article history:
Received 8 May 2025
Revised 12 November 2025
Accepted 21 November 2025
Available online 22 November 2025

Keywords:
9,9′-Spirobifluorenes
Organic light-emitting diodes
Host materials
Emitters
Electron-transport materials
Hole-transport materials
C–H arylation

ABSTRACT

9,9′-Spirobifluorene (SBF) derivatives, as a unique class of conjugated frameworks, have been extensively investigated in the field of organic electronics. The introduction of diverse substituents to various positions on SBF can modulate the photoelectric properties of SBF derivatives. Multisite substitution endows SBF derivatives with structural diversity, thus providing more opportunities for adjusting the photoelectric properties of materials. However, the synthesis of multi-substituted SBFs is more difficult, and their structure-activity relationships are also more unpredictable. This review focuses on multi-substituted SBFs, detailing their synthesis methods, photoelectric properties, thermal stabilities, and applications in organic light-emitting diodes (OLEDs). Multi-substituted SBFs are typically synthesized using multi-halogenated or multi-boronate ester-substituted SBF precursors. In addition, transition metal-catalyzed C–H arylation reactions represent an exceptionally efficient approach for preparing multi-substituted SBFs. The effects of the type, number, and position of substituents on the thermal stability, photophysical and electrochemical properties, and carrier mobility of these SBF derivatives are systematically reviewed. Their roles as emitters, hosts, electron-transport materials, and hole-transport materials in OLED devices are summarized and discussed.

© 2026 Published by Elsevier B.V. on behalf of Chinese Chemical Society and Institute of Materia Medica, Chinese Academy of Medical Sciences.

1. Introduction

Spiro-conjugated compounds consist of two or more π-systems linked by a shared sp^3-hybridized atom, and this unique structural feature makes them one of the most important classes of organic semiconductors [1,2]. Among these compounds, 9,9′-spirobifluorene (SBF), which comprises two fluorene rings connected through a shared spirocarbon atom, has attracted considerable attention in the field of organic electronics [3,4]. SBF fragments are extensively employed in organic light-emitting diodes (OLEDs) [5], organic photovoltaics (OPVs) [6–9], organic field-effect transistors (OFETs) [10,11], and organic lasers [12]. In OLEDs, SBF derivatives can serve as emitters [13], host materials [14,15], electron-transport materials [16], and hole-transport materials [17], and have showcased excellent device performance.

Common OLED devices are composed of a multilayer structure, and each organic layer must meet specific requirements to ensure optimal device performance. The host material in the emitting layer (EML) must satisfy two key requirements: first, it should have a higher triplet energy (E_T) than the dopant to ensure efficient energy transfer; second, it needs to exhibit high and balanced carrier mobilities [18]. The dopant, as another key component of the EML, should feature high quantum efficiency and an appropriate emission wavelength [19]. The hole transport layer (HTL) must demonstrate high hole mobility to ensure efficient carrier transport and have a suitably aligned highest occupied molecular orbital (HOMO) with respect to the adjacent layers, thereby minimizing the energy barrier for hole injection [20]. The electron transport layer (ETL) should exhibit excellent electron mobility and feature a lowest unoccupied molecular orbital (LUMO) that is appropriately aligned with those of the emitting layer and the cathode [21]. Additionally, it must possess a higher E_T than the emitting materials to effectively prevent triplet excitons in the emitting layer from leaking into the ETL. Furthermore, all these materials must exhibit outstanding thermal and morphological stabilities to minimize the possibility of phase separation during heating, which is conducive to forming homogeneous and stable amorphous films *via* thermal evaporation during the OLED fabrication process and significantly enhancing the operational lifetime of the device [22].

* Corresponding authors.
E-mail addresses: zhengliu0827@hbnu.edu.cn (Z. Liu), gdyin@hbnu.edu.cn (G. Yin), jingbolan@scu.edu.cn (J. Lan).

https://doi.org/10.1016/j.cclet.2025.112155
1001-8417/© 2026 Published by Elsevier B.V. on behalf of Chinese Chemical Society and Institute of Materia Medica, Chinese Academy of Medical Sciences.

These stringent requirements have been driving the development of novel molecular structures for OLED applications.

The two fluorene units of the SBF fragment are arranged on orthogonal planes, causing the molecules to occupy a larger three-dimensional space in the solid state. This mutually perpendicular configuration facilitates the inhibition of strong intermolecular interactions [1], thereby suppressing the formation of aggregates and excimers and preventing exciton quenching caused by tight molecular packing. As a result, the luminescence quantum efficiency of the target materials is substantially improved [23,24]. The introduction of the spirolinkage has also been shown to enhance the morphological stability of the material and effectively extend device lifetime [25]. Additionally, the molecular structure characteristics of conjugation breaking and rigid-flexible combination, introduced by the sp^3 carbon atom, endow the material with higher E_T [26]. In recent years, incorporating the spirostructure into organic functional molecules has emerged as a pivotal research focus. Numerous new materials based on the spiroconjugated structure have been designed and synthesized, and their three-dimensional structures, molecular stacking, photophysical and electrochemical properties have been systematically investigated [27].

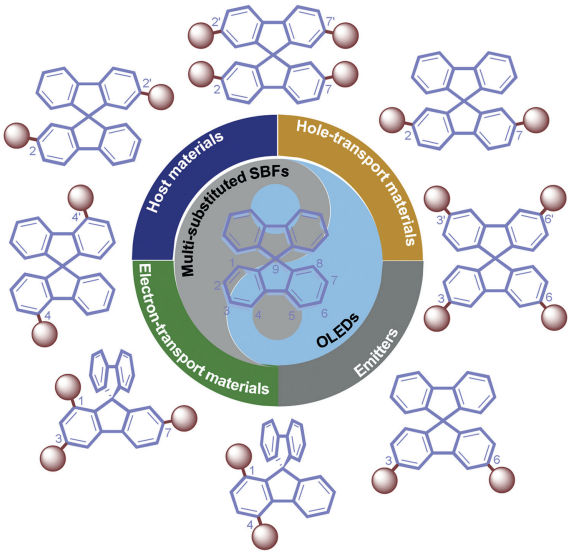
The synthesis of SBF can be traced back to 1930 [28]. Clarkson and Gomberg prepared [1,1′-biphenyl]−2-ylmagnesium iodide from 2-iodo-1,1′-biphenyl and Mg. The Grignard reagent underwent nucleophilic addition with 9*H*-fluoren-9-one, followed by intramolecular Friedel-Crafts alkylation, yielding SBF in a total yield of 59%. Alternatively, (1,1′-biphenyl)-2-yllithium generated from ^{n}BuLi and 2-bromobiphenyl can serve as a substitute for the Grignard reagent in nucleophilic addition reactions [29]. This two-step synthesis method is currently the main approach to access organic optoelectronic materials based on the SBF core fragment.

The introduction of substituents to the different sites on the SBF skeleton can modulate photoelectric properties of SBFs, thereby influencing the performance of OLED devices [30]. Cyril Poriel *et al.* have carried out many studies and presented relevant reviews on introducing a phenyl substituent to different sites of the SBF backbone [31,32]. The incorporation of the phenyl group to the C1 position of SBF increases the decomposition temperature (T_d) to 272 °C and alters the glass transition temperature (T_g) to 66 °C. The installation of the phenyl group to the C2 position of SBF would significantly reduce E_T to 2.55 eV. Introducing the phenyl group to the C3 position enhances the fluorescence quantum yield (Φ_f) to 0.74. Moreover, when the phenyl ring is located at the C4 position of SBF, the maximum emission wavelength is bathochromically shifted to 359 nm.

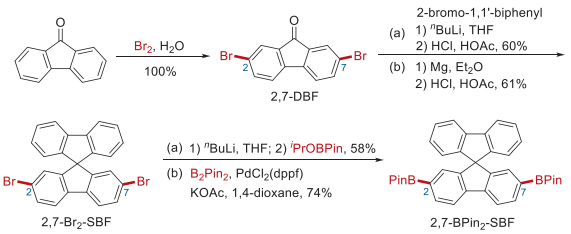
Multisite substitution endows SBF derivatives with structural diversity, thus providing more opportunities for adjusting the photoelectric properties of materials. However, the synthesis of multi-substituted SBFs is more difficult, and their structure-activity relationships are also more unpredictable. In recent years, a considerable number of multi-substituted SBFs have been reported and applied in OLED devices. Herein, the effects of multiple substituents on the thermal stability, photophysical and electrochemical properties, as well as the carrier mobility of these SBF derivatives are systematically reviewed, and their performances when applied as emitters, hosts, electron-transport materials and hole-transport materials in OLED devices are summarized and discussed (Scheme 1).

2. Multi-substituted SBFs with C2 substitution

The substituent at the C2 position of SBF is positioned just at the *para*-position of the biphenyl unit, and the *para*-linkage enables the maximization of π-conjugation extension, thereby leading to a low E_T. Mono-substituted SBFs bearing phenyl [30], pyrimidinyl [33], diphenylamine [34], carbazole [35], dibenzothiophene



Scheme 1. Substitution patterns of multi-substituted SBFs and their applications in OLEDs.



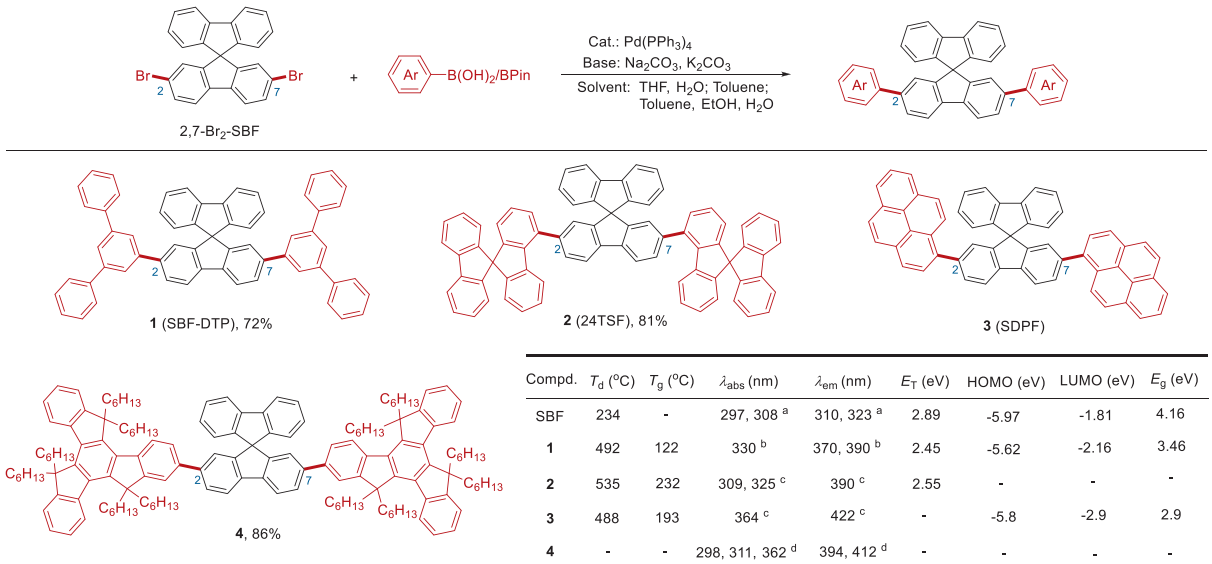
Scheme 2. Synthesis of 2,7-Br_2-SBF and 2,7-$BPin_2$-SBF.

[36], dibenzofuran [37], and 9,9′-spirobifluorene [38] at the C2 position have been successfully synthesized *via* coupling reactions involving 2–bromo or 2-boronate ester substituted SBF precursors.

2,7-Disubstituted SBFs are typically applied as luminescent materials, which are usually derived from the significant precursor 2,7-dibromo-9,9′-spirobifluorene (2,7-Br_2-SBF) (Scheme 2). 2,7-Br_2-SBF was synthesized through the electrophilic bromination of 9*H*-fluoren-9-one [39], followed by nucleophilic addition using either (1,1′-biphenyl)-2-yllithium [40] or (1,1′-biphenyl)-2-ylmagnesium bromide [41], and subsequent intramolecular Friedel-Crafts alkylation-type spiroannulation. The boronate ester 2,7-$Bpin_2$-SBF is also an important precursor, which was synthesized in 58% yield from the reaction with ^{i}PrOBPin after the lithium-halide exchange of 2,7-Br_2-SBF with ^{n}BuLi [42]. 2,7-Br_2-SBF can also be rapidly converted to 2,7-$Bpin_2$-SBF through a Miyaura borylation reaction [16].

Four SBF derivatives (**1**–**4**), substituted by aromatic rings at C2 and C7 positions, were prepared in yields ranging from 72% to 86% *via* the Suzuki-Miyaura reaction of 2,7-Br_2-SBF with corresponding aryl boronic acids or boronic esters (Scheme 3) [43–46]. The typical reaction conditions involve $Pd(PPh_3)_4$ as the catalyst, Na_2CO_3 or K_2CO_3 as the base, and solvents such as toluene, a tetrahydrofuran (THF)/H_2O mixture, or a toluene/EtOH/H_2O mixture.

The operation life of OLEDs remains one of the most important parameters in the current development stage, especially for blue OLED devices. C–H and C–C bonds have higher bond energies than C–X (X = O, N, P, S) bonds. Therefore, pure hydrocarbon (PHC) host materials are generally considered more stable compared to heteroatom-containing hosts. The development of next-generation host materials that exclude heteroatoms has emerged as a promising strategy [47,48]. In 2024, Liao and Jiang *et al.* developed the



Compd.	T_d (°C)	T_g (°C)	λ_{abs} (nm)	λ_{em} (nm)	E_T (eV)	HOMO (eV)	LUMO (eV)	E_g (eV)
SBF	234	-	297, 308 [a]	310, 323 [a]	2.89	-5.97	-1.81	4.16
1	492	122	330 [b]	370, 390 [b]	2.45	-5.62	-2.16	3.46
2	535	232	309, 325 [c]	390 [c]	2.55	-	-	-
3	488	193	364 [c]	422 [c]	-	-5.8	-2.9	2.9
4	-	-	298, 311, 362 [d]	394, 412 [d]	-	-	-	-

Scheme 3. Synthesis of 2,7-substituted SBFs (**1**–**4**) and their thermal, photophysical, and electrochemical properties. [a] In cyclohexane. [b] In toluene. [c] In DCM. [d] In the solid film.

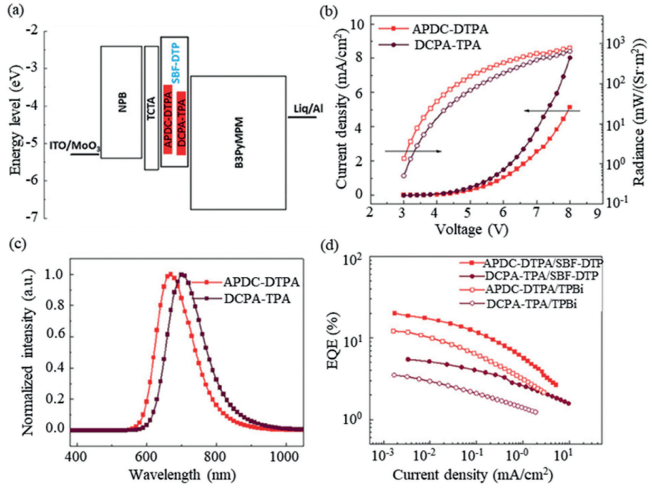
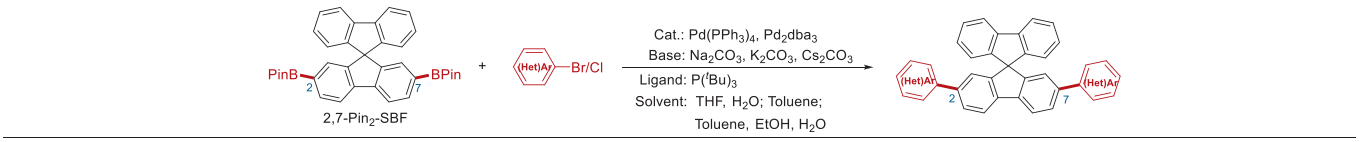


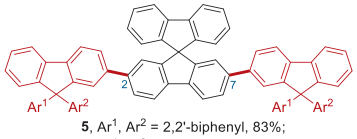
Fig. 1. The configuration and performance of OLED devices based on **1** (SBF-DTP). Reproduced with permission [43]. Copyright 2024, John Wiley & Sons, Inc.

PHC host **1** (SBF-DTP) by introducing two 1,1′:3′,1′′-terphenyl (TP) units at the C2,7 positions of SBF framework (Scheme 3) [43]. **1** exhibits excellent thermal and morphological stability with a T_d of 492 °C and a T_g of 122 °C. The introduction of two TP units significantly enhances the T_d value compared to SBF (T_d = 234 °C). The maximum emission wavelength of **1** in toluene is 330 nm, and a wide optical bandgap (E_g) of 3.46 eV was measured from its absorption spectrum. Due to the extended π-conjugation at C2 and C7 positions of SBF, the E_T of **1** reduces from 2.89 eV for SBF to 2.45 eV. Although the E_T value is relatively low, it is sufficient for use as the host material for red emitters, such as APDC-DTPA (E_T = 2.02 eV) [49] and DCPA-TPA (E_T = 1.48 eV) [50]. The HOMO/LUMO energy levels of **1** are −5.62/−2.16 eV. The single crystal structure of **1** exhibits a loose stacking mode attributed to its mutually perpendicular spatial configuration. The OLED devices using **1** as the host were fabricated with the device configuration: ITO/MoO_3 (5 nm)/NPB (30 nm)/TCTA (10 nm)/ the emitting layer (EML) (20 nm)/B_3PyMPM (70 nm)/Liq (2 nm)/Al (120 nm) (Fig. 1a). The device, doped with red-emitting thermally activated delayed fluorescence (TADF) emitter APDC-DTPA (5 wt%) as the EML, exhibits a high maximum external quantum efficiency (EQE_{max}) of 20.03 %, with an electroluminescence peak (λ_{EL}) at 670 nm. Meanwhile, the device doped with fluorescence emitter DCPA-TPA (5 wt%) as the EML exhibits an EQE_{max} of 5.47 % with deep red-light emission (λ_{EL} = 702 nm) (Fig. 1). The good device performance suggests that developing spirobased PHC host materials could be an effective strategy for achieving high-performance OLEDs with deep red-light emission.

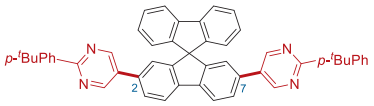
In 2009, Ma and Yang *et al.* synthesized oligo-9,9′-spirobifluorene **2** (24TSF) with a C2/C4′′-linkage of SBF (Scheme 3) [44]. **2** exhibits excellent thermal properties with a high T_d (535 °C) and a high T_g (232 °C) attributed to its rigid spirostructure. The E_T of 2.55 eV indicates that **2** can act as host for the green emitter Ir(ppy)$_3$ (E_T = 2.42 eV), as well as the red emitter (ppq)$_2$Ir(acac) (E_T = 2.01 eV) in PhOLEDs [51]. The device incorporating Ir(ppy)$_3$ as the phosphor displays an EQE_{max} of 12.6 %, a maximum current efficiency (CE_{max}) of 48.2 cd/A, and a maximum power efficiency (PE_{max}) of 26.8 lm/W. The device using (ppq)$_2$Ir(acac) as the phosphor demonstrates an EQE_{max} of 10.5 %, a CE_{max} of 8.4 cd/A, and a PE_{max} of 4.1 lm/W. This is the first time that C2/C4′′-linked oligo-SBF derivative was applied as the host of PhOLEDs, paving the way for the development of SBFs with C4 substitution as the host materials.

The introduction of diverse chromophores to the C2 and C7 positions of SBF also represents a promising strategy for the development of highly efficient luminescent materials. For instance, 2,7-di(pyren-1-yl)-9,9′-spirobifluorene (denoted as SDPF, compound **3**) shows a blue emission peak at 422 nm in CH_2Cl_2 solution, with a Φ_f as high as 0.78 [45]. **3** also demonstrates excellent thermal stability, with a T_d of 488 °C and a T_g of 193 °C. A non-doped blue-light-emitting OLED employing **3** as both host and emitter achieves a CE_{max} of 4.9 cd/A with a CIE coordinate of x = 0.17, y = 0.27. The PL spectrum of π-conjugated molecule **4**, which is constructed from two truxene units linked by SBF, shows two characteristic emission peaks at 394 and 412 nm, accompanied by a shoulder at approximately 440 nm [46]. Compound **4** exhibits a narrow full width at half-maximum (FWHM) of approximately 50 nm. Furthermore, a series of SBF derivatives (**5**–**12**), substituted with spirorings or nitrogen-containing heterocycles (such as pyrimidine and triazine) at the C2 and C7 positions, can also be synthesized as emitters with excellent luminescent properties *via* Suzuki-Miyaura

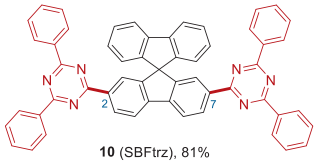




5, Ar^1, Ar^2 = 2,2'-biphenyl, 83%;
6, Ar^1, Ar^2 = Ph, 68%;
7, Ar^1, Ar^2 = *p*-Tol, 63%;
8, Ar^1 = *p*-Tol, Ar^2 = Naphthalen-1-yl, 86%

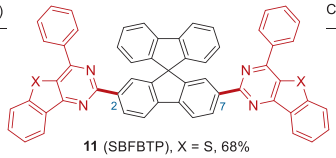


9 (TBPSF), 94%



10 (SBFtrz), 81%

Compd.	T_d (°C)	T_g (°C)	λ_{abs} (nm) [a]	λ_{em} (nm) [a]	HOMO (eV)	LUMO (eV)
5	450	no	353	393, 412, 441	-5.58	-2.16
6	425	201	353	393, 412, 438	-5.57	-2.06
7	435	210	353	394, 414, 440	-5.57	-2.07
8	430	231	356	395, 415, 441	-5.56	-2.14



11 (SBFBTP), X = S, 68%
12 (SBFBFP), X = O, 61%

Compd.	T_d (°C)	T_g (°C)	λ_{abs} (nm)	λ_{em} (nm)	E_T (eV)	HOMO (eV)	LUMO (eV)
9	420	195	350 [a] (350) [b]	390, 410 [a] (430) [b]	-	-	-
10	492	-	338 [c]	430 [c]	2.53	-6.68	-3.49
11	467	-	391 [c]	405 [c]	2.43	-6.58	-3.41
12	439	-	383 [c]	405 [c]	2.47	-6.52	-3.29

Scheme 4. Synthesis of 2,7-substituted SBFs (**5**–**12**) and their thermal, photophysical, and electrochemical properties. [a] In $CHCl_3$. [b] In the solid film. [c] In THF.

reactions, when employing 2,7-$BPin_2$-SBF and various halogenated aromatic hydrocarbons as substrates (Scheme 4) [16,52,53].

The ter(9,9′-diarylfluorene)s (**5**–**8**), with different aryl substituents, all have excellent thermal stability with T_d reaching up to 450 °C (Scheme 4) [52]. Compounds **6**–**8** exhibit different T_g, ranging from 189 °C to 231 °C. The attachment of different aryl groups to the spirocarbon has a negligible impact on the electronic properties, leading to similar UV–vis absorption and PL spectra for these ter(9,9′-diarylfluorene)s in $CHCl_3$ solution. Compounds **5**–**8** demonstrate exceptional optical performance and their Φ_f in ethyl acetate solution are up to 99%. In solid thin films, Φ_f are 90% for **5**, 82% for **6**, 87% for **7**, and 66% for **8**, respectively. The blue OLED device employing compound **5** as the emitter exhibits a threshold voltage (V_{on}) of ~3 V, an EQE of 2.5%–3%, and a brightness over 5000 cd/m^2. These results collectively indicate that diaryl-substituted SBFs at the C2 and C7 positions are highly promising candidates as emitters for blue OLEDs.

The SBF derivative **9** (TBPSF), substituted with electron-deficient pyrimidine at C2,7 positions, was developed as both an emitter and a host material [53]. In $CHCl_3$ solution, the blue light-emitting **9** exhibits maximum emission wavelengths at 390 and 410 nm, with a high Φ_f up to 100%. In thin films, the maximum emission wavelength is bathochromically shifted to 440 nm with a Φ_f of 80%. Furthermore, **9** demonstrates favorable thermal stability, with a T_g of 195 °C and a T_d of 420 °C. Blue OLEDs with the configuration of ITO/PEDT:PSS/NCB/**9** or **9** and perylene (1 wt%)/Alq_3/LiF/Al were fabricated. The non-doped device displays a maximum brightness exceeding 30,000 cd/m^2, while the doped device reaches a maximum brightness of approximately 80,000 cd/m^2.

In addition, introducing electron transport units, such as pyrimidine or triazine, into the C2 and C7 positions of SBF is conducive to the development of electron transport materials (ETMs) for OLEDs with high electron mobility [16]. For example, **10** (SBFTrz), **11** (SBFBTP), and **12** (SBFBFP) possess excellent thermal stability, owing to robust molecular structure and the C–H···N hydrogen bonding between nitrogen-containing heterocycles and the SBF core. The T_d of **10**, **11**, and **12** are 492, 467, and 439 °C, respectively (Scheme 4). The higher E_T values of **10** (2.53 eV), **11** (2.43 eV), and **12** (2.47 eV) than that of green phosphorescent $Ir(ppy)_3$ (E_T = 2.42 eV) favor blocking exciton from leakage into the ETL in green PhOLEDs [54]. The low electron density of these compounds results in relatively low LUMO energy levels for **10** (−3.49 eV), **11** (−3.41 eV), and **12** (−3.29 eV). The PhOLED devices, using **10**, **11**, **12**, or DBFTrz (2,8-bis(4,6-diphenyl-1,3,5-triazin-2-yl)dibenzo[*b*,*d*]furan, as the reference) as the ETL, exhibit EQE_{max} values of 20.5%, 19.2%, 20.5%, and 20.3%, respectively (Fig. 2). Moreover, the devices based on **10** and **12** have a longer lifetime than those based on DBFTrz. The combination of the SBF core with the electron transport units provides opportunities for the development of novel ETLs with good electron transport properties.

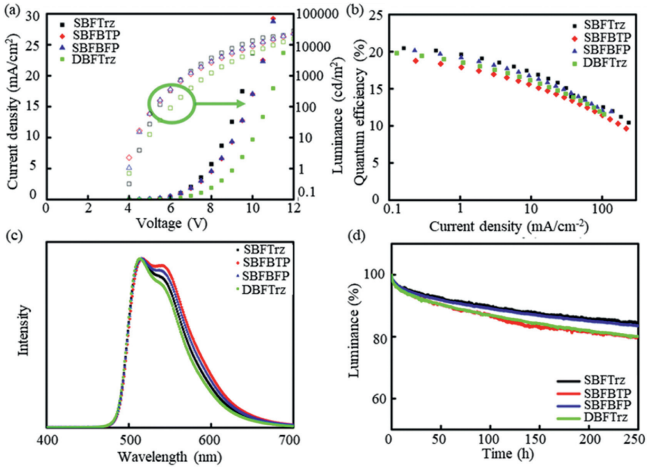
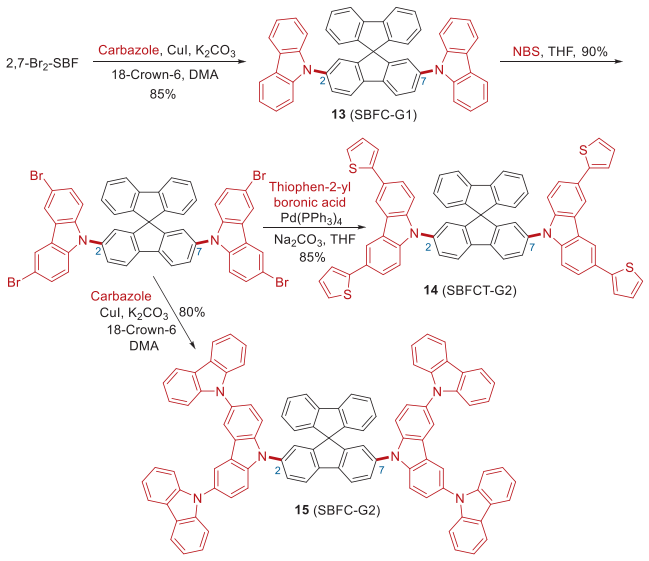


Fig. 2. The performance of PhOLEDs based on **10** (SBFTrz), **11** (SBFBTP), **12** (SBFBFP), and DBFTrz. Reproduced with permission [16]. Copyright 2022, The Royal Society of Chemistry.

Similarly, the introduction of electron-donating substituents endows the resulting SBFs with excellent hole transport properties. The carbazole-substituted SBF derivative **13** (SBFC-G1) was synthesized *via* the Ullmann reaction, employing 2,7-Br_2-SBF and carbazole as substrates (Scheme 5) [55]. Subsequent electrophilic bromination of **13** with excess NBS yielded the tetra–bromo intermediate in 90% yield. Further transformations of bromine atoms afforded **14** (SBFCT-G2) and **15** (SBFC-G2). **13**, **14**, and **15** exhibit excellent thermal properties, with T_d ranging from 587 °C to 650 °C and T_g ranging from 174 °C to 227 °C. **14** (λ_{max} = 387 nm) and **15** (λ_{max} = 388 nm) display a bathochromic shift of the emission spectra compared to **13** (λ_{max} = 367 nm), attributed to the ex-



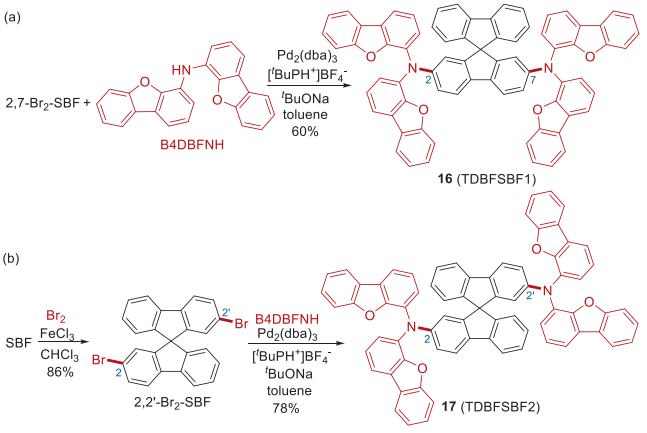
Compd.	T_d (°C)	T_g (°C)	λ_{abs} (nm) [a]	λ_{em} (nm) [a]	Φ_f (%)[a]	HOMO (eV)	LUMO (eV)	E_g (eV)
13	587	174	334	367	50	-5.67	-2.31	3.36
14	650	-	343	387	11	-5.57	-2.33	3.24
15	617	227	318, 341	388	11	-5.40	-2.22	3.18

Scheme 5. Synthesis of 2,7-substituted SBFs (**13**–**15**) and their thermal, photophysical, and electrochemical properties. [a] In $CHCl_3$.

tended π-conjugation system. The HOMO/LUMO energy levels of **13**, **14**, and **15** are −5.59/−2.23, −5.45/−2.21, and −5.36/−2.18 eV, respectively. When employed as the HTL in OLED devices, **14** and **15** exhibited maximum luminance values of 23,100 and 25,400 cd/m^2, respectively.

Two SBFs substituted with bis(dibenzofuran-4-yl)amine groups (B4DBFNH) at C2,7 and C2,2′ positions (denoted as TDBFSBF1 and TDBFSBF2, compounds **16** and **17**, respectively) have also been synthesized as HTMs for PhOLEDs [56]. **16** was obtained in 60 % yield *via* the Buchwald-Hartwig amination between 2,7-Br_2-SBF and B4DBFNH (Scheme 6a). 2,2′-Br_2-SBF, a key intermediate for the synthesis of 2,2′-substituted SBFs, was prepared in 88 % yield *via* electrophilic bromination of SBF using Br_2 as an electrophilic reagent [57], and subsequent amination gave **17** in 78 % yield (Scheme 6b). The large molecular weight (1010 g/mol) endows compounds **16** (T_d = 540 °C, T_g = 178 °C) and **17** (T_d = 524 °C, T_g = 188 °C) with excellent thermal stabilities. The extension of π-conjugation in **16**, featuring two bis(dibenzofuran-4-yl)amine groups on the same fluorene core, results in a lower E_T of 2.5 eV compared to that of **17**. The high hole mobility (u_h) values of **16** and **17** were measured to be 1.2×10^{-4} and 1.9×10^{-3} cm^2 V^{-1} s^{-1}, respectively. The green PhOLED device, with **16** as the HTL, presents an EQE at 1000 cd/m^2 (EQE_{1000}) of 22 %, a V_{on} of 2.30 V, and a LT_{50} of 89,000 h. Under identical conditions, **17** exhibits a slightly lower EQE of 21.4 %, a higher V_{on} of 2.55 V, and a shorter LT_{50} of 76,000 h (Fig. 3). These results indicate that introducing substituents to distinct positions of SBF is an effective strategy for developing high-performance hole-transport materials.

A typical OLED is composed of multiple functional layers. The increase in the number of functional layers will lead to an increase in the manufacturing cost of the device and a decrease in the qualification rate [58]. To simplify the device architecture of typical PhOLEDs, a trisubstituted SBF derivative **18** (2,7-DiCbz-SBF-4′-$POPh_2$) bearing both electron-donating groups (EDG) and an electron-withdrawing group (EWG), was designed and synthe-



Compd.	T_d (°C)	T_g (°C)	λ_{abs} (nm) [a]	λ_{em} (nm) [a]	E_T (eV)	HOMO (eV) [b]	LUMO (eV) [b]	E_g (eV) [c]
16	540	178	350	405	2.5	-4.99	-1.43	3.0
17	524	188	375	405, 420	2.6	-5.20	-1.45	3.2

Scheme 6. Synthesis of SBFs (**16** and **17**) and their thermal and photophysical properties. [a] In the solid film. [b] From DFT calculations. [c] Calculated from the oneset of the absorption spectra.

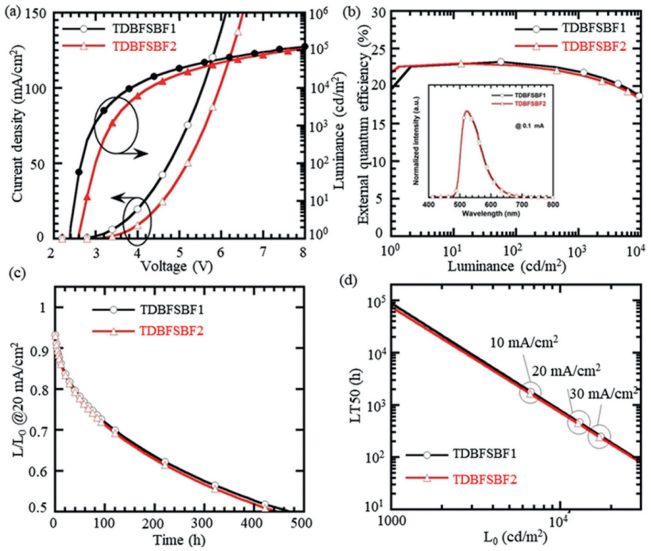
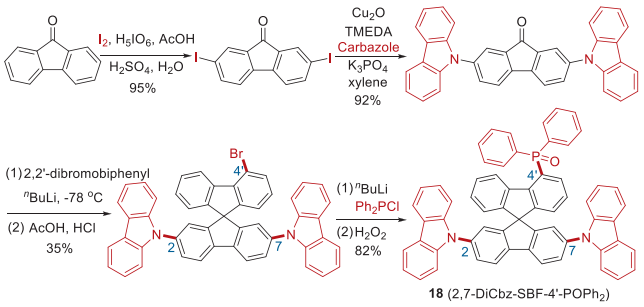


Fig. 3. The performance of PhOLEDs based on **16** (TDBFSBF1) and **17** (TDBFSBF2). Reproduced with permission [56]. Copyright 2022, John Wiley & Sons, Inc.

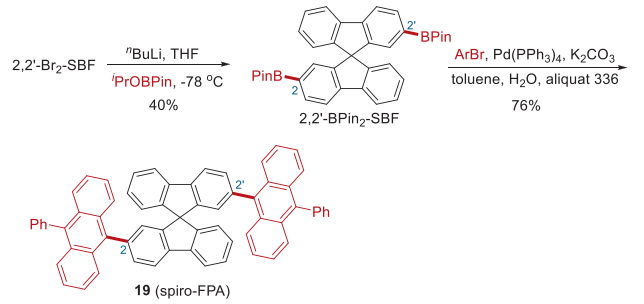
sized (Scheme 7) [59]. However, the introduction of different functional groups into the SBF framework prevents the direct use of substrates containing multiple halogen substitutions, which is primarily caused by the challenge of achieving chemical selectivity at different anchor points. After introducing the first type of functional group, an additional bromine atom is introduced to the C4′-position during the construction of the spiroring by using a brominated lithium reagent. Initially, the electrophilic iodination of fluorenone followed by the Ullmann reaction with carbazole yielded 2,7-di(9*H*-carbazol-9-yl)-9*H*-fluoren-9-one. Subsequently, a nucleophilic addition and intramolecular Friedel-Crafts spiroannulation afforded 2,7,4′-trisubstituted SBF. The lithiated intermediate obtained *via* lithium-halogen exchange was then trapped with Ph_2PCl and oxidized with H_2O_2 to give **18**.

The investigation of the thermal properties revealed that the 2,7,4′-trisubstituted SBF **18** exhibits remarkable thermal stability with a T_d of 426 °C and a T_g of 193 °C (Scheme 7). Compared



Compd.	T_d (°C)	T_g (°C)	λ_{abs} (nm) [a]	λ_{em} (nm) [a]	E_T (eV)	HOMO (eV)	LUMO (eV)	E_g (eV)
18	426	193	292, 349	362, 380	2.64	-5.51	-2.10	3.41

Scheme 7. Synthesis of **18** and its thermal, photophysical, and electrochemical properties. [a] In cyclohexane.

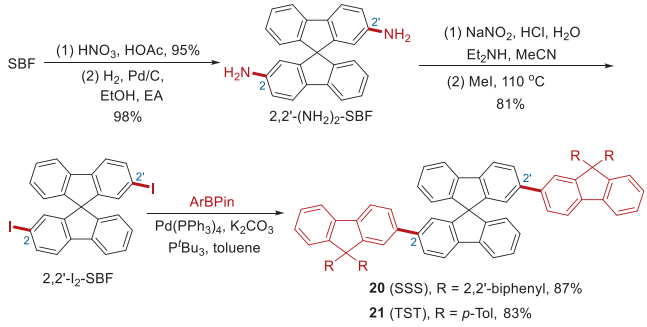


Compd.	T_d (°C)	T_g (°C)	λ_{abs} (nm) [a]	λ_{em} (nm) [a]	HOMO (eV)	LUMO (eV)	E_g (eV)
19	450	223	375, 397	425	-5.47	-2.45	3.02

Scheme 8. Synthesis of **19** and its thermal, photophysical, and electrochemical properties. [a] In toluene.

with compound **13** [55], the introduction of the diphenylphosphine oxide group at the C4 position of SBF reduces the T_d and increases the T_g. **18** is an efficient violet-blue fluorophore with a maximum emission wavelength of 362, 380 nm and a high Φ_f of 0.78. The HOMO and LUMO energy levels of **18** are −5.51 and −2.10 eV, respectively. The π-conjugation disruption between fluorene unit and the sterically hindered phosphine oxide group endows **18** with a similarly low E_T (2.64 eV) to that of compound **13**. Subsequently, a single-layer PhOLED device was prepared with structure of ITO/PEDOT:PSS/**18**:Ir(ppy)$_3$ (10%)/LiF/Al, where **18** serves as the host material for the green phosphorescent emitter Ir(ppy)$_3$ (E_T = 2.42 eV). The single-layer device demonstrates favorable performance characteristics, exhibiting an EQE_{max} of 13.2%, a maximum luminance of approximately 20,000 cd/m^2, a CE_{max} of 45.8 cd/A, a PE_{max} of 49.6 lm/W, and a low V_{on} of 2.4 V.

2,2′-Substituted SBFs (**19**–**21**) have also been synthesized and applied in OLEDs [60,61]. Initially, 2,2′-Br$_2$-SBF underwent a lithium-halide exchange reaction with ^{n}BuLi, and the resulting lithiated intermediate was trapped by ^{i}PrOBPin to afford 2,2′-BPin$_2$-SBF, a diboronic ester-substituted derivative of SBF. Subsequently, 2,2′-BPin$_2$-SBF was coupled with 9–bromo–10-phenylanthracene *via* the Suzuki-Miyaura reaction to yield the 9,9′-spirobifluorene-linked bisanthracene **19** (spiroFPA) in 76% yield (Scheme 8) [60]. **19** possesses a high T_d of 450 °C and a high T_g of 223 °C. The toluene solution of **19** displays blue fluorescence (λ_{max} = 425 nm). The HOMO/LUMO energy levels of **19** are −5.47 and −2.45 eV, respectively. A blue electroluminescent device with an emitting layer consisting of 1.0 wt% 2,5,8,11-tetra–*tert*–butylperylene doped in **19** exhibits a luminescence efficiency of 4.9 cd/A.



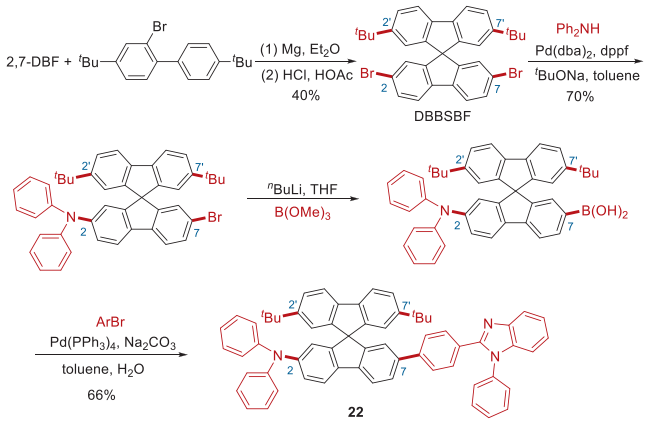
Compd.	T_d (°C)	T_g (°C)	λ_{abs} (nm) [a]	λ_{em} (nm) [a]	E_T (eV)	HOMO (eV)	LUMO (eV)
20	464	228	310, 333	367, 387	2.28	-5.72	-2.08
21	475	197	333	370, 387	2.28	-5.73	-2.09

Scheme 9. Synthesis of 2,2′-substituted SBFs (**20** and **21**) and their thermal, photophysical, and electrochemical properties. [a] In $CHCl_3$.

In 2005, Chung-chih Wu *et al.* applied PHC small molecules as host materials in phosphorescent OLEDs (Scheme 9) [61]. **20** (SSS) and **21** (TST), featuring two substituents of 9,9′-spirofluorene located at the C2,2′-positions, were synthesized using 2,2′-I$_2$-SBF as a key intermediate. Unlike the direct electrophilic bromination of SBF to produce 2,2′-Br$_2$-SBF, the electrophilic iodination of the aromatic ring usually has low reactivity. Therefore, 2,2′-I$_2$-SBF was synthesized *via* electrophilic nitration of SBF, followed by reduction and Sandmeyer reaction [62]. The Suzuki-Miyaura coupling reaction of 2,2′-I$_2$-SBF with aryl boronic esters afforded **20** and **21** with yields of 87% and 83%, respectively. Compared to the positional isomers **5** and **7**, **20** and **21** exhibit higher T_d of 464 and 475 °C, respectively. However, the T_g of compound **21** decreases to 197 °C. **20** and **21** exhibit similar emission spectra (λ_{max} = 367, 387 nm and 370, 387 nm, respectively). The *para*-linkage with efficient π-conjugation extension results in lower E_T of 2.28 eV for both **20** and **21**. OLED devices using **20** and **21** as the emitting materials exhibit UV-light emission with EL peaks at 373 and 393 nm, respectively. Limited by their low E_T, **20** and **21** are only suitable as host materials for red phosphorescent emitters. The hosts **20** and **21** display EQE_{max} of 8.6% and 10%, respectively, with low V_{on} of 2.5–3.0 V.

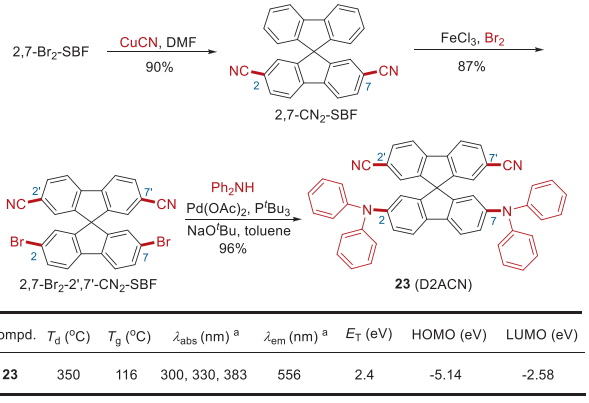
The ambipolar transport material **22** was designed and synthesized by introducing benzimidazole and diphenylamine groups into the SBF framework [63,64]. 2,7-Dibromo-2′,7′-di–*tert*–butyl–9,9′-spirobifluorene (DBBSBF) was prepared in 40% yield *via* a nucleophilic addition reaction of (4,4′-di–*tert*–butyl–[1,1′-biphenyl]–2-yl)magnesium bromide with 2,7-DBF, followed by an intramolecular cyclization reaction (Scheme 10). The diphenylamine and benzimidazole functional groups were introduced through the Buchwald-Hartwig amination and Suzuki-Miyaura coupling. The T_d and T_g of **22** reach 467 and 170 °C, respectively, indicating its excellent thermal and morphological stability. **22** exhibits blue emission in both toluene solution and thin films, with Φ_f of 76% and 72%, respectively. The E_T of **22** is as low as 2.3 eV. The u_h and u_e values are 1.17×10^{-5} cm^2 V^{-1} s^{-1} and 2.38×10^{-5} cm^2 V^{-1} s^{-1}, respectively, demonstrating an effective bipolar carrier transport property of **22**. When employed as either the emitting or host material in OLEDs, **22** enables devices to achieve EQEs of 1.4% and 6.9%, respectively.

Furthermore, the introduction of electron-rich diphenylamino and electron-deficient cyano moieties into the two respective biphenyl branches of an SBF core enables the development of



Compd.	T_d (°C)	T_g (°C)	λ_{abs} (nm) [a]	λ_{em} (nm) [a]	E_T (eV)	HOMO (eV)	LUMO (eV)
22	467	170	315, 376	475	2.30	-5.21	-2.21

Scheme 10. Synthesis of **22** and its thermal, photophysical, and electrochemical properties. [a] In toluene.

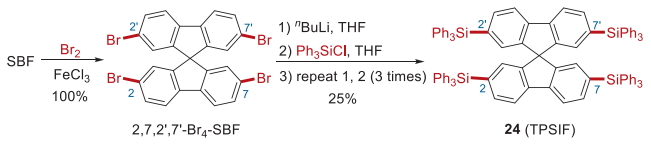


Compd.	T_d (°C)	T_g (°C)	λ_{abs} (nm) [a]	λ_{em} (nm) [a]	E_T (eV)	HOMO (eV)	LUMO (eV)
23	350	116	300, 330, 383	556	2.4	-5.14	-2.58

Scheme 11. Synthesis of **23** and its thermal, photophysical, and electrochemical properties. [a] In the solid film.

ambipolar host material **23** (D2ACN) (Scheme 11) [65]. Hung and Wong *et al.* synthesized 9,9′-spirobifluorene-2,7-dicarbonitrile (2,7-CN_2-SBF) in 90% yield *via* a copper-promoted substitution reaction between 2,7-Br_2-SBF and CuCN. Subsequently, an electrophilic bromination followed by Buchwald-Hartwig amination with diphenylamine afforded **23** [66]. Compound **23** exhibits a high T_d of 350 °C and a T_g of 116 °C. The maximum absorption wavelengths of **23** are 300, 330, and 338 nm, while its thin films display weak fluorescence emission peaking at 556 nm. The HOMO/LUMO energy levels of **23** are −5.14/−2.58 eV. **23** has a balanced bipolar charge transport capability with similar values of u_h and u_e. **23** has a low E_T of 2.4 eV, making it suitable as a host material for red phosphorescent emitters. And the red-emitting PhOLED device using **23** as the host material presents an EQE_{max} of 10.8%.

Considering the reduction in E_T caused by π-conjugation extension, the introduction of π-conjugation-disrupting functional groups represents an effective strategy for preserving a high E_T. In 2021, the SBF derivative **24** (TPSiF), featuring four triphenylsilyl substituents at the C2,2′,7,7′ positions, was synthesized and applied as a universal host material for red, green, and blue (RGB) PhOLEDs (Scheme 12) [67]. In the presence of excess Br_2, SBF underwent a quadruple bromination reaction to give 2,2′,7,7′-tetrabromo-9,9′-spirobifluorene (2,2′,7,7′-Br_4-SBF) in quantitative yield [57], which underwent lithium-halide exchange with ^{n}BuLi



Compd.	T_d (°C)	T_g (°C)	λ_{abs} (nm) [a]	λ_{em} (nm) [a]	E_T (eV)	HOMO (eV)	LUMO (eV)
24	539	135	323	343	2.79	-5.96	-2.31

Scheme 12. Synthesis of **24** and its thermal, photophysical, and electrochemical properties. [a] In toluene.

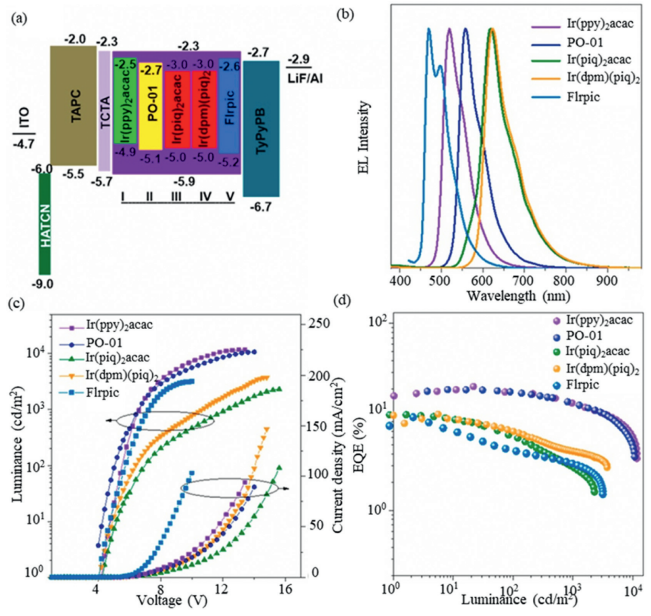
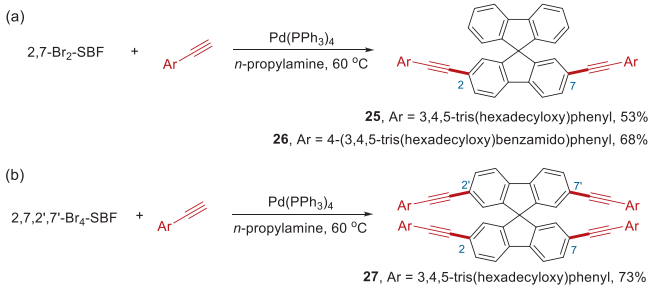


Fig. 4. The configuration and performance of PhOLEDs based on **24** (TPSiF). Reproduced with permission [67]. Copyright 2021, Elsevier B.V.

and nucleophilic substitutions to triphenylsilyl chloride, affording **24** in a relatively low yield (25%).

The introduction of triphenylsilyl groups makes the T_d of **24** greatly increased to 539 °C. The maximum absorption and emission wavelengths of **24** are 324 and 341 nm, respectively. Furthermore, the E_g between HOMO and LUMO is 3.65 eV. The introduction of triphenylsilyl groups at the C2 positions of SBF slightly reduces the E_T, yet **24** retains a high E_T value of 2.79 eV. The PhOLEDs with iridium complexes ($Ir(ppy)_2acac$, PO-01, $Ir(piq)_2acac$, $Ir(dpm)(piq)_2$, and FIrpic) as luminescent materials were sequentially prepared to investigate the electroluminescence performance of **24** as a host, and the device configuration was as follows: ITO/HATCN (5 nm)/TAPC (50 nm)/TCTA (5 nm)/5 wt% iridium complexes: **24** (20 nm)/TmPyPB (40 nm)/LiF (1 nm)/Al (Fig. 4). These devices exhibit pure emission from the luminescent materials with the EL peaks at 520, 558, 620, 470, and 470 nm, and EQE_{max} of 21.1%, 19.5%, 10.5%, 10.7%, and 10.0%, respectively. Although the substituent groups are positioned at the C2 and C7 sites, the conjugation interruption at the Si center endows the material with a remarkably high E_T level. This unique property thus enables it to serve as a versatile host material for PhOLEDs with emission wavelengths spanning from blue to red.

Furthermore, SBFs bearing C2-alkynyl substituents also exhibit good luminescent properties [68]. Alkyne-substituted SBFs could be synthesized through Sonagashira coupling reactions, where halogenated SBFs and aryl alkynes were utilized as substrates. When 2,7-Br_2-SBF was employed as the substrate, 2,7-substituted SBFs **25** and **26** were obtained in yields of 53% and 68%, respec-



Compd.	λ_{abs} (nm) [a]	λ_{em} (nm) [a]	Φ_f (%) [a]	λ_{em} (nm) [b]	Φ_f (%) [b]
25	329, 363, 378	396, 417	72	476	33
26	329, 366, 383	395, 417	22	448	11
27	363, 378	397, 420	85	456	41
28	365, 383	396, 417	32	450	30

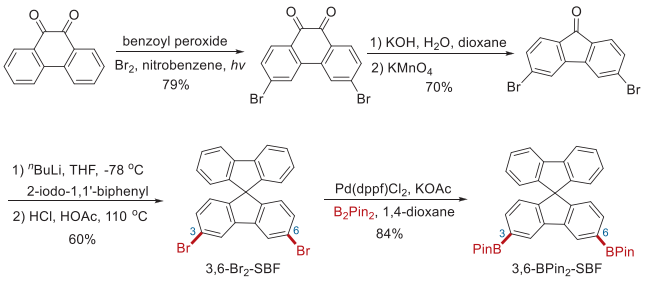
Scheme 13. Synthesis of 2,2′-substituted SBFs (**25** and **26**), 2,2′,7,7′-substituted SBFs (**27** and **28**), and their photophysical properties. [a] In cyclohexane. [b] In the solid film.

tively (Scheme 13a). When 2,2′,7,7′-Br_4-SBF served as the substrate, the tetra-substituted SBFs **27** and **28** could also be obtained in yields of 73 % and 80 %, respectively (Scheme 13b). Compound **25** (λ_{max} = 329, 363, 278 nm) exhibits a red-shifted maximum absorption wavelength compared to mono-alkynyl substituted 2-((3,4,5-tris(hexadecyloxy)phenyl)ethynyl)-9,9′-spirobifluorene (λ_{max} = 332, 349 nm), which is attributed to the extension of π-conjugation induced by the presence of two ethynyl-3,4,5-tris(hexadecyloxy)benzene moieties. In cyclohexane, the maximum emission wavelengths of these multi-substituted SBFs are approximately 396 and 417 nm, with quantum yields ranging from 22 % to 85 %, which indicates that the ethynyl-benzene/fluorene/ethynyl-benzene moiety can serve as an efficient blue emitter. In solid films, compound **27** exhibits a maximum emission wavelength of 456 nm, and its quantum yield reaches 41 %.

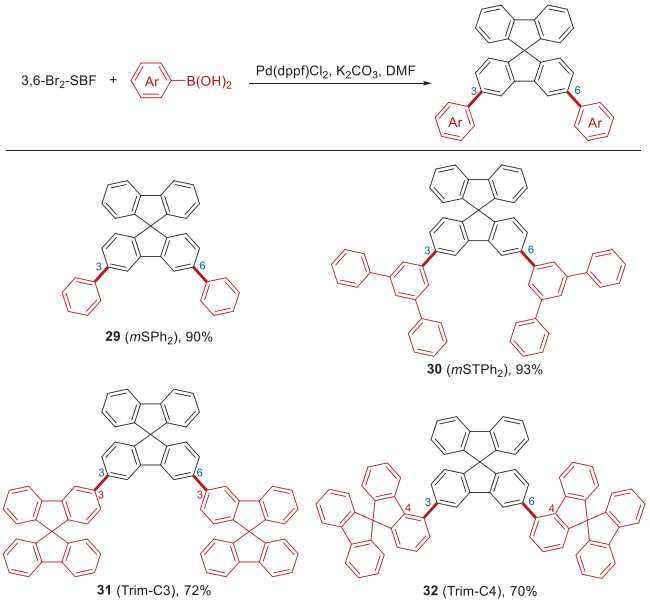
The introduction of various groups with different electronic properties has a significant impact on the properties of the resulting molecules, owing to the maximization of π-conjugation extension between the groups at the C2 position and the SBF skeleton. When electron-donating groups are incorporated at 2,7-positions, SBFs can function as hole transport materials. Conversely, upon introduction of electron-withdrawing groups, SBFs usually serve as electron transport materials. Moreover, the incorporation of chromophores endows SBFs with the ability to act as luminescent materials. However, grafting multiple substituents at the C2-position results in relatively low E_T, which is disadvantageous for their applications as host materials. Significantly, the 2,7-substituted SBFs (substituents on the same fluorene core) exert a more pronounced electronic effect compared to the 2,2′-substituted SBFs (substituents on different fluorene cores).

3. Multi-substituted SBFs with C3 substitution

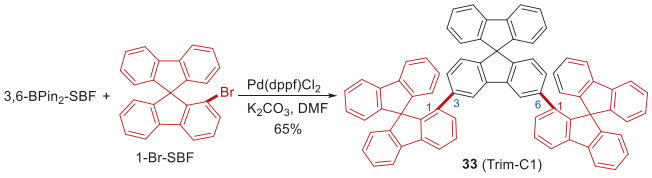
The electronic effect of the *meta*-linkage leads to the disruption of π-conjugation of SBFs substituted at the C3 position. Consequently, SBFs with C3 substitution represent a promising choice for high E_T host materials. Mono-substituted SBFs, featuring a variety of functional groups, such as phenyl [30], phosphine oxide [69], phenyl carbazole [70], and 9,9′-spirobifluorene [71] at the C3 position, have been synthesized and utilized as host materials in OLEDs. These explorations provide insight into the structure-



Scheme 14. Synthesis of 3,6-Br_2-SBF and 3,6-$BPin_2$-SBF.



Scheme 15. Synthesis of 3,6-substituted SBFs (**29**–**32**) by 3,6-Br_2-SBF.



Scheme 16. Synthesis of **33** by 3,6-$BPin_2$-SBF.

activity relationships of multi-substituted SBFs with C3 substitution.

The key intermediates for the synthesis of 3,6-substituted 9,9′-spirobifluorene derivatives are 3,6-dibromo-9,9′-spirobifluorene (3,6-Br_2-SBF) and 3,6-bis(4,4,5,5-tetramethyl-1,3,2-dioxaborolan-2-yl)-9,9′-spirobifluorene (3,6-$BPin_2$-SBF) (Scheme 14) [72,73]. These intermediates were obtained through the transformation of 3,6-dibromo-9*H*-fluoren-9-one, which was produced *via* a bromination/oxidation sequence of phenanthrene-9,10–dione. The introduction of phenyl (**29**, *m*SPh_2), *meta*-terphenyl (**30**, *m*$STPh_2$), 9,9′-spirobifluorene-3-yl (**31**, Trim-C3), and 9,9′-spirobifluorene-4-yl (**32**, Trim-C4) to the C3,6 positions of SBF can be achieved through Suzuki-Miyaura coupling between 3,6-Br_2-SBF and the corresponding aryl boronic acid or boronate ester (Scheme 15) [73,74]. However, the Suzuki-Miyaura reaction between 3,6-Br_2-SBF and 1-Bpin-SBF failed due to the high steric hindrance at the C1 position of the SBF ring. **33** (Trim-C1) was successfully synthesized with a yield of 68 % by employing 3,6-$Bpin_2$-SBF and 1-Br-SBF as substrates (Scheme 16) [73].

Table 1
Thermal, photophysical, and electrochemical properties of multi-substituted SBFs with C3 substitution (**29**–**37**).

Property	T_d (°C)	T_g (°C)	λ_{abs} (nm)	λ_{em} (nm)	Φ_f (%)	E_T (eV)	HOMO (eV)	LUMO (eV)	E_g (eV)	μ_h ($cm^2\ V^{-1}\ s^{-1}$)	μ_e ($cm^2\ V^{-1}\ s^{-1}$)
29 (mSPh$_2$) [a]	287	126	311, 325	339, 352	-	2.79	−5.89	−1.94	3.95	2.25×10^{-8}	0.49×10^{-8}
30 (mSTPh$_2$) [a]	407	176	310, 324	345, 358	-	2.79	−5.99	−2.08	3.91	3.08×10^{-8}	8.59×10^{-8}
31 (Trim-C3) [b]	548	248	309	345	82	2.73	−5.90	−1.98	3.92	3.43×10^{-9}	5.06×10^{-9}
32 (Trim-C4) [b]	515	233	308	365	65	2.75	−5.97	−2.06	3.91	1.06×10^{-8}	1.27×10^{-8}
33 (Trim-C1) [b]	482	198	310	325	56	2.84	−5.88	−1.83	4.05	8.41×10^{-8}	0.225×10^{-8}
34 (3,6-DDTA-SBF) [a]	413	169	310	401	-	2.68	−5.20	−2.11	3.09	2.53×10^{-2}	-
35 (3,3′-DDTA-SBF) [a]	430	145	313	401	-	2.75	−5.20	−3.08	3.12	1.61×10^{-2}	-
36 (3,3′, 6,6′-DDTA-SBF) [a]	506	-	311	402	-	2.66	−5.20	−3.08	3.07	3.83×10^{-2}	-
37 (3,3-dimtp-SBF) [b]	490	172	306, 316	338	60	2.82	−5.97	−2.09	3.88	8.75×10^{-6}	2.52×10^{-6}

The UV–vis absorption spectra, emission spectra, and quantum yields were measured in toluene [a] and cyclohexane [b].

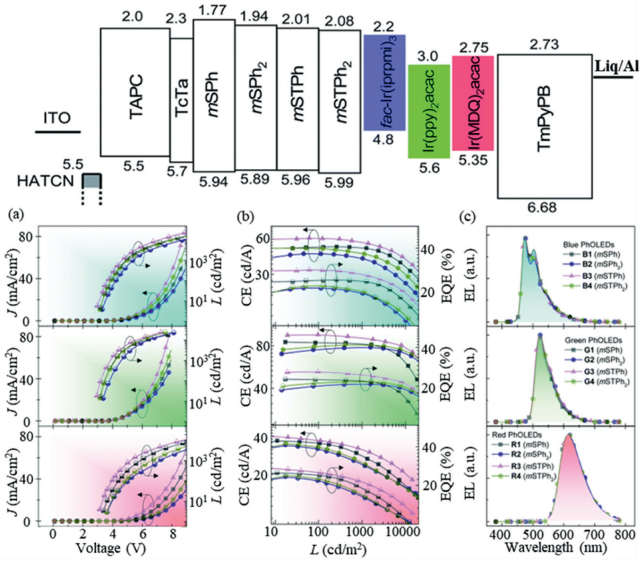


Fig. 5. The configuration and performance of PhOLEDs based on **29** (mSPh$_2$), **30** (mSTPh$_2$), *m*SPh, and *m*STPh. Reproduced with permission [74]. Copyright 2020, The Royal Society of Chemistry.

29 and **30** both exhibit high thermal stability, with T_d values of 287 and 407 °C, respectively [74]. Moreover, they possess excellent morphological stability, with T_g values of 126 and 176 °C, respectively (Table 1). These properties represent an improvement compared to those of the corresponding C3 monoaryl-substituted SBF derivatives, 3-phenyl-9,9′-spirobifluorene (*m*SPh, $T_d = 262$ °C, $T_g = 90$ °C) and 3-(*meta*-terphenyl)-9,9′-spirobifluorene (*m*STPh, $T_d = 318$ °C, $T_g = 133$ °C). **29** ($\lambda_{max} = 311$, 325 nm) and **30** ($\lambda_{max} = 310$, 324 nm) display similar UV–vis absorption profiles, with maximum emission wavelengths of 339, 352 nm and 345, 358 nm, respectively. The slight bathochromic shift in the emission bands from *m*SPh (335, 348 nm) to **29**, and from *m*STPh (344, 356 nm) to **30**, results from the extension of the π-conjugation. Compared with mono-substituted compounds *m*SPh ($E_T = 2.82$ eV) and *m*STPh ($E_T = 2.82$ eV), the introduction of two aryl groups at the C3,6 positions of SBF slightly decreases the E_T values of **29** and **30** to 2.79 eV. The HOMO/LUMO energy levels of **29** and **30** are −5.89/−1.94 eV and −5.99/−2.08 eV, respectively. Given the high E_T and suitable energy levels, **29**, **30**, *m*SPh, and *m*STPh have been utilized as host materials in RGB PhOLEDs (Fig. 5). Both the green and red PhOLED devices achieve EQE$_{max}$ exceeding 20%. For the blue devices, hosts **29** and **30** exhibit EQE$_{max}$ of 19.6% and 20.4%, respectively. Notably, compound **30** stands out as one of the most efficient universal hosts for RGB PhOLEDs, further demonstrating the significant potential of multi-substituted SBFs in boosting the comprehensive performance of OLEDs.

Zhou and Poriel *et al.* designed three PHC host materials by assembling three SBF units. The SBF trimers **31** (Trim-C3), **32** (Trim-C4), and **33** (Trim-C1) exhibit high T_d of 548, 515 and 482 °C, respectively (Table 1) [73]. The T_g values are all above 200 °C (256 °C for **31**, 241 °C for **32**, and 205 °C for **33**). These data indicate that the three isomers possess significantly enhanced thermal and morphological stability. The maximum absorption wavelengths of **31** and **32** are 309 and 308 nm, respectively, with both exhibiting a shoulder peak at longer wavelengths. **32** has a larger extension of the π-conjugation according to the stronger shoulder band in the absorption profile. **33** displays a similar UV–vis absorption profile to SBF, with a peak of 310 nm. The introduction of two 9,9′-spirobifluorene-1-yl groups at the C3,6 positions of SBF has minimal impact on the absorption spectrum. This phenomenon can be attributed to the effective disruption of the π-conjugation among the three SBF units, which results from the combined influence of a robust steric hindrance and a *meta*-terphenyl linkage.

Compared with SBF ($\lambda_{max} = 310$, 323 nm), the maximum emission wavelength of **31**, **32**, and **33** are bathochromic-shifted to 345, 365, and 325 nm, respectively. The most efficient disruption of π-conjugation between the 9,9′-spirobifluorene-1-yl group and 9,9′-spirobifluorene-3-yl group results in **33** having a higher E_T value of 2.84 eV compared to **31** (2.75 eV) and **32** (2.73 eV). The HOMO/LUMO energy levels are −5.90/−1.98 eV for **31**, −5.97/−2.06 eV for **32**, and −5.88/−1.83 eV for **33**. The corresponding E_g values are 3.92, 3.91, and 4.05 eV, respectively, which facilitate effective charge recombination within the emitters. The charge carrier mobilities of the three isomers appear to be well balanced. The blue PhOLED, employing **33** as host, exhibits an exceptionally high EQE$_{max}$ of 24.1%, a V_{on} of 2.56 V, a CE$_{max}$ of 50 cd/A, and a PE$_{max}$ of 44.1 lm/W. In addition, **33** demonstrates superior stability with a low-efficiency roll-off with an EQE of 17.9% at 1000 cd/m^2. When using **31** and **32** as host materials, EQE$_{max}$ values of 9.6% and 20.5% are observed, respectively (Fig. 6).

By taking advantage of the electronic decoupling effect arising from the *meta*-linkage mode between the SBF fragment and functional groups, several efficient HTMs (**34**–**36**) were designed by introducing di-4-tolylamino groups at the C3,6 positions of the SBF core. 3,6-Di(*N*,*N*-ditolylamino)-9,9′-spirobifluorene **34** (3,6-DDTA-SBF) was synthesized *via* the Buchwald-Hartwig amination of 3,6-Br$_2$-SBF and di-*p*-tolylamine in 75% yield (Scheme 17a) [75]. Introducing multiple halogen atoms into the non-electrophilic reaction sites on distinct fluorene rings of the SBF framework remains a challenge. Utilizing *pseudo*-halogen groups as substitutes for halogen atoms to enable further derivatization is a practical synthetic strategy. **35** and **36** were prepared through a deliberated synthetic route. The key intermediate 3,3′-Cl$_2$–6,6′-OMe$_2$-SBF was prepared through chelation-assisted Pd-catalyzed *ortho*-C–H diarylation followed by intramolecular Friedel-Crafts alkylation (Scheme 17b). The Buchwald-Hartwig amination of 3,3′-Cl$_2$–6,6′-OMe$_2$-SBF with di-*p*-tolylamine, followed by deprotection and esterification reactions, afforded 3,3′-DDTA-6,6′-OTf$_2$-SBF. The fur-

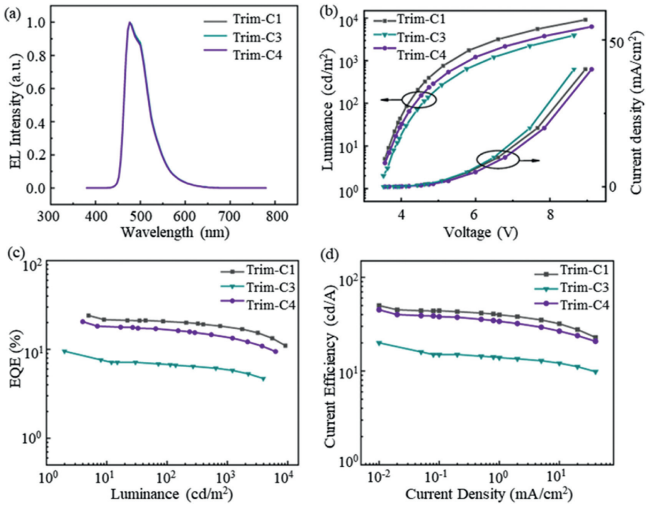
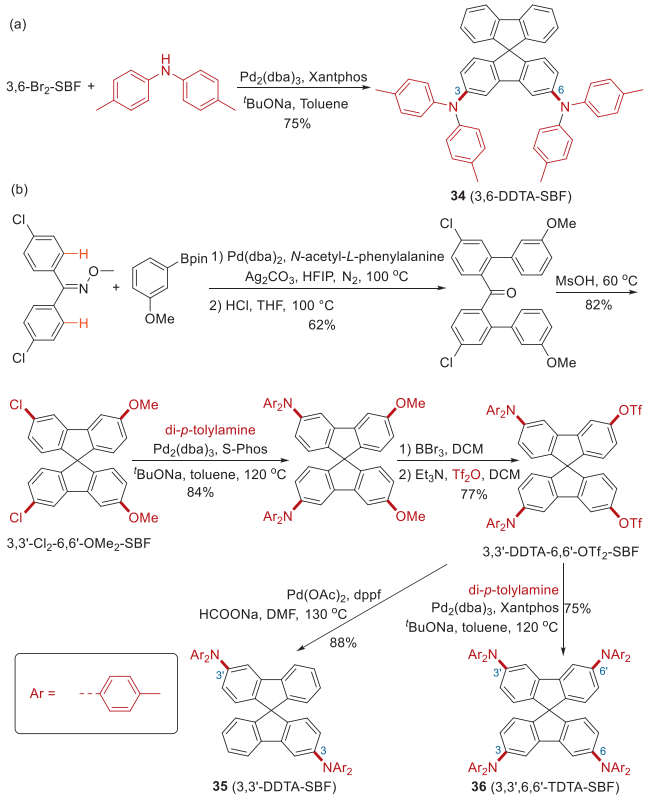


Fig. 6. The performance of PhOLEDs based on **31** (Trim-C3), **32** (Trim-C4), and **33** (Trim-C1). Reproduced with permission [73]. Copyright 2024, John Wiley & Sons, Inc.



Scheme 17. Synthesis of **34**, **35**, and **36**.

ther transformation of trifluoromethanesulfonate groups produced **35** (3,3′-DDTA-SBF) and **36** (3,3′,6,6′-TDTA-SBF). The high T_d values of **34** (413 °C), **35** (430 °C), and **36** (506 °C) indicate their excellent thermal stability (Table 1). These compounds also exhibit excellent morphological stability, with high T_g of 169 °C and 145 °C for **34** and **35**, respectively. While the number of diarylamino substituents varies among these compounds, the SBF-based triarylamine derivatives display identical UV–vis absorption spectra with a peak at 310 nm and emission spectra with a peak at 401 nm. Despite the incorporation of strong electron-donating di-4-tolylamino groups, the high E_T values are maintained at 2.68 eV for **34**, 2.75 eV

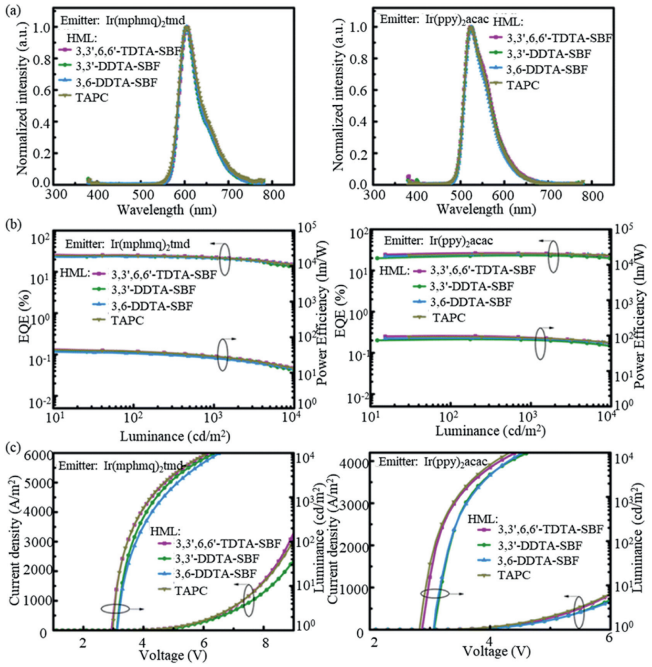


Fig. 7. The performance of red and green PhOLEDs based on **34** (3,6-DDTA-SBF), **35** (3,3′-DDTA-SBF), **36** (3,3′,6,6′-TDTA-SBF), and TAPC. Reproduced with permission [75]. Copyright 2024, The Royal Society of Chemistry.

for **35**, and 2.66 eV for **36**, owing to the electronic decoupling effect of the *meta*-linkage. The high hole mobilities (u_h) of **34** (2.53×10^{-2} cm^2 V^{-1} s^{-1}), **35** (1.61×10^{-2} cm^2 V^{-1} s^{-1}), and **36** (3.83×10^{-2} cm^2 V^{-1} s^{-1}), which are comparable to those of 1,1-bis(4-*N*,*N*-ditolylaminophenyl)cyclohexane (TAPC) (3.84×10^{-2} cm^2 V^{-1} s^{-1}), one of the most classical HTMs, highlight their excellent hole-transporting properties. **34**, **35**, **36**, and the reference TAPC were employed as HTMs in RGB PhOLEDs. The red devices exhibit EQE_{max} values of 24.0 % for **34**, 23.9 % for **35**, 26.1 % for **36**, and 25.1 % for TAPC, with an EL peak at 605 nm (Fig. 7). Among green devices, **36** exhibits the highest EQE_{max} of 26.4 %. The blue PhOLED devices, incorporating **34**, **35**, **36**, or TAPC as the HTM and FIrpic as the emitter material, display EQE_{max} values of 24.0 %, 23.9 %, 26.1 %, and 25.1 %, respectively (Fig. 8). Furthermore, when using the boron-nitrogen-based multiple resonance (BN-MR) material BCz-BN as the emitter and FIrpic as the sensitizer, the OLED device with **36** as the HTM achieves a high EQE_{max} of 29.8 %. The development of these high-performance HTMs underscores the significance of multi-substituted SBFs at C3 substitutions for assembling high-performance RGB OLEDs.

To further enhance the efficiency of OLED devices and mitigate efficiency roll-off, Poriel, Jiang, and Zhou *et al.* recently reported a novel PHC host material, which is based on the multi-substituted SBF skeleton applied in phosphorescence-sensitized multi-resonance thermally activated delayed fluorescence (MR-TADF) OLEDs (Scheme 18) [76]. 2-Iodo-4-bromobiphenyl was initially synthesized from 2-amino-4-bromobiphenyl *via* the Sandmeyer reaction. Subsequently, a selective lithium-iodide exchange took place instead of a lithium-bromide exchange under ^{n}BuLi, leading to the formation of the corresponding lithiated intermediate. This intermediate then underwent a nucleophilic attack on 3–bromo–9*H*-fluoren-9-one followed by a spiroannulation, ultimately resulting in the production of 3,3-Br_2-SBF. Finally, 3,3-Br_2-SBF was efficiently coupled with (3,5-diphenylphenyl)boronic acid, affording **37** (3,3-dimtp-SBF) in 79 % yield. Compared to the positional isomer **30** (T_d = 407 °C, T_g = 176 °C) [74], the T_d of **37** has a significant increase to 490 °C, while the T_g has a slight decrease to 172

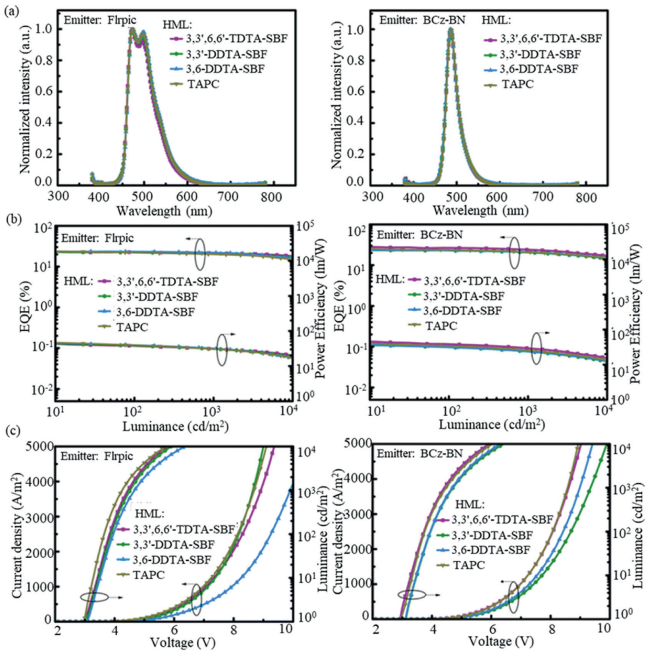
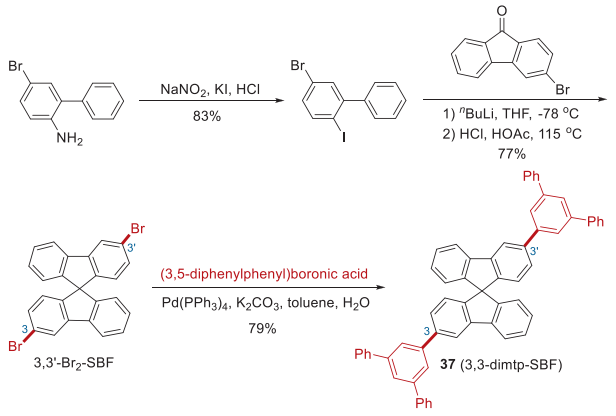


Fig. 8. The performance of blue PhOLEDs and BN-MR OLEDs based on **34** (3,6-DDTA-SBF), **35** (3,3′-DDTA-SBF), **36** (3,3′,6,6′-TDTA-SBF), and TAPC. Reproduced with permission [75]. Copyright 2024, The Royal Society of Chemistry.



Scheme 18. Synthesis of **37** by 3,3′-Br_2-SBF.

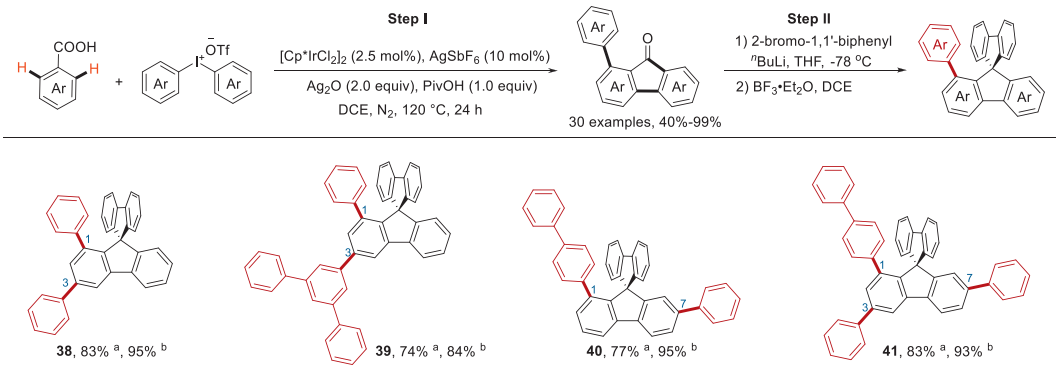
°C (Table 1). Furthermore, the higher E_T (2.82 eV) is attributed to the reduction of π-conjugation caused by the connection of *meta*-terphenyl fragments on different fluorene rings. The HOMO and LUMO energy levels of **37** are −5.97 eV and −2.09 eV, respectively, resulting in a wide E_g of 3.88 eV. The OLED devices using **37** as the host were fabricated with the device configuration: ITO/HATCN (10 nm)/TAPC (40 nm)/TCTA (10 nm)/mCP (10 nm)/emitting layer (20 nm)/TmPyPB (40 nm)/Liq (2 nm)/Al (80 nm). The device incorporating the phosphorescent material FIrpic (10 wt%) as a sensitizer for DtBuCzB (2 wt%) demonstrates a high EQE_{max} of 29.3 %. When fac-Ir(tpz)$_3$ (20 wt%) was employed as the sensitizer, the device exhibited a high EQE_{max} of 31.0 % and an outstanding low efficiency roll-off of 23.3 % at high luminance levels of 1000 cd/m^2. The application of PHC material as the host in phosphorescence-sensitized MR-TADF OLEDs provides a viable strategy for fabricating high-performance devices.

The multi-substituted SBFs at the C3,3′ and C3,6 positions generally exhibit high E_T due to the disruption of π-conjugation, among which the substitution pattern at the C3,3′ position has a smaller impact than that at the C3,6 position. The properties of the high E_T are favorable for multi-substituted SBFs with C3 substitution serving as the host material in OLEDs. Moreover, the incorporation of electron-donating groups at the C3,3′, C3,6, or even C3,3′,6,6′ positions of the SBF fragment has enabled SBFs to emerge as high-performance hole transport materials.

4. Multi-substituted SBFs with C1 substitution

Multi-substituted SBFs with C1 substitution possess the characteristics of *meta*-linkage and the large steric effect between the C1 substitution and the SBF core. This combination leads to the π-conjugation being completely broken, thereby maintaining a high E_T value. Mono-substituted SBFs with C1 substitution, such as methyl [77], carbazole [78], phenyl [30], biaryl [79], polycyclic aryl [80], and 9,9′-spirobifluorene [81] have been synthesized and further investigated in terms of the physical and electronic properties. These studies also point out the direction for the development of multi-substituted SBFs featuring C1 substitution.

Given that the C1 position of SBF is not an electrophilic reaction site, it is not possible to directly introduce functional groups at the C1 position *via* electrophilic halogenation. The synthesis of C1 mono-substituted SBFs generally entails multi-step procedures and suffers from relatively low yields. The construction of multi-substituted SBFs bearing C1 substituent poses an even greater challenge [82]. To efficiently introduce an aryl group at the C1 position of SBF, You and Lan *et al.* developed a highly efficient protocol for the diarylation/annulation of benzoic acids with diaryliodonium salts (Ph_2IOTf) (Scheme 19). Their research demonstrates that $Pd(OAc)_2$ and $[Cp^*RhCl_2]_2/AgSbF_6$ can catalyze this diarylation/annulation reaction, but with lower yields compared to $[Cp^*IrCl_2]_2/AgSbF_6$. The one-pot transformation was ultimately accomplished under the conditions in which $[Cp^*IrCl_2]_2/AgSbF_6$ served as the catalyst, Ag_2O as the oxidant, and PivOH as the additive in TFE at 120 °C under N_2 atmosphere. The *in situ* generation of trifluoromethane sulfonic acid (HOTf) by PivOH and Ph_2IOTf promotes this intramolecular Friedel-Crafts acylation. This reaction exhibits excellent functional group tolerance (30 examples, 40 %–99 %) and proceeds smoothly on a scale of 3.0 mmol. This rapid and concise strategy significantly streamlines access to a series of multi-aryl fluorenones. The spirofluorene unit was ultimately introduced through a classical sequence involving a nucleophilic addition reaction between multi-aryl fluorenones and the lithiated biphenyl, followed by an intramolecular cyclization reaction. Additionally, 1,3,7-triphenyl-9,9′-spirobifluorene (**42**) was constructed *via* a five-step traditional synthetic method (Scheme 20). These multi-aryl SBF derivatives display high thermal and morphological stability, with T_d ranging from 288 °C to 415 °C and T_g values ranging from 110 °C to 172 °C (Table 2). Compared to 3-(*meta*-terphenyl)-9,9′-spirobifluorene (*m*STPh, T_d = 318 °C, T_g = 133 °C) [43], the elevated T_d (415 °C) and T_g (172 °C) values for **39** indicate that the introduction of the C1 phenyl group enhances the thermal properties of the SBF skeleton. The bathochromically shifted emissions of compounds **41** (λ_{max} = 346, 361 nm) and **42** (λ_{max} = 345, 360 nm) are mainly attributed to the extension of π-conjugation at the C7 position. The E_T values of these multi-aryl SBF derivatives are 2.83 eV for **38**, 2.82 eV for **39**, 2.57 eV for **40**, 2.49 eV for **41**, and 2.57 eV for **42**. The π-conjugation extension at the C7 position results in a lower E_T for compounds **40**, **41**, and **42**, which exhibit approximate E_T values with 2-phenyl-9,9′-spirobifluorene (2.56 eV) [30]. The introduction of the C1 biphenyl group leads to relatively high mobilities of **40** ($u_h = 1.29 \times 10^{-6}$ cm^2 V^{-1} s^{-1}, $u_e = 9.32 \times 10^{-6}$ cm^2 V^{-1} s^{-1}) and **41** ($u_h = 1.51 \times 10^{-6}$ cm^2 V^{-1} s^{-1}, $u_e = 1.26 \times 10^{-6}$ cm^2 V^{-1} s^{-1}). Owing to their E_T levels, these multi-aryl SBF derivatives were employed as the host materials for RGB PhOLEDs (Fig. 9). In the blue PhOLED devices, hosts **38** and **39** exhibit EQE_{max} values of 18.6 % and 17.5 %, respectively. Green



Scheme 19. Synthesis of multi-substituted SBFs (**38**–**41**) with C1 substitution by diarylation/annulation of benzoic acids. Isolated yield of step I [a] and step II [b].

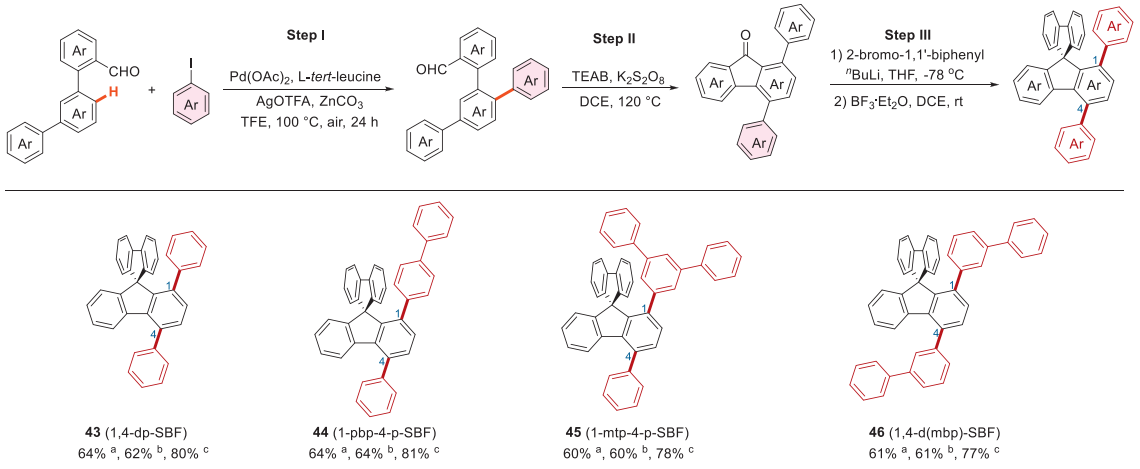
Table 2
Thermal, photophysical, and electrochemical properties of multi-substituted SBFs with C1 substitution (**38**–**48**).

Property	T_d (°C)	T_g (°C)	λ_{abs} (nm)	λ_{em} (nm)	Φ_f (%)	E_T (eV)	HOMO (eV)	LUMO (eV)	E_g (eV)	μ_h ($cm^2\ V^{-1}\ s^{-1}$)	μ_e ($cm^2\ V^{-1}\ s^{-1}$)
38 [a]	288	-	298, 310, 319	339, 350	45	2.83	−5.76	−2.05	3.71	2.9×10^{-7}	3.0×10^{-7}
39 [a]	415	172	298, 310, 319	345, 356	72	2.82	−5.82	−2.09	3.73	2.3×10^{-7}	1.2×10^{-6}
40 [a]	339	110	298, 310, 322	338, 355, 370	75	2.57	−5.79	−2.14	3.65	1.29×10^{-6}	9.32×10^{-6}
41 [a]	341	140	298, 311, 329	346, 361	72	2.49	−5.75	−2.17	3.58	1.51×10^{-6}	1.26×10^{-6}
42 [a]	363	-	298, 310, 329	345, 360	67	2.57	−5.75	−2.16	3.59	2.5×10^{-7}	2.2×10^{-7}
43 (1,4-dp-SBF) [a]	304	78	298, 310	384	43	2.75	−5.77	−1.74	3.92	1.29×10^{-5}	2.74×10^{-5}
44 (1-pbp-4-p-SBF) [a]	356	97	298, 310	385	52	2.75	−5.79	−1.75	3.90	3.83×10^{-5}	4.06×10^{-5}
45 (1-mtp-4-p-SBF) [a]	380	-	298, 311	386	47	2.75	−5.77	−1.77	3.88	1.45×10^{-5}	3.15×10^{-5}
46 (1,4-d(mbp)-SBF) [a]	394	100	298, 311	386	55	2.81	−5.78	−1.77	3.89	1.84×10^{-5}	1.63×10^{-5}
47 (1,6-dimtp-SBF) [b]	435	150	311, 318	338	65	2.83	−5.93	−2.08	3.85	9.26×10^{-6}	4.04×10^{-6}
48 (1,8-dimtp-SBF) [b]	407	127	312	317, 332	24	2.86	−5.84	−1.93	3.91	6.94×10^{-6}	3.23×10^{-6}

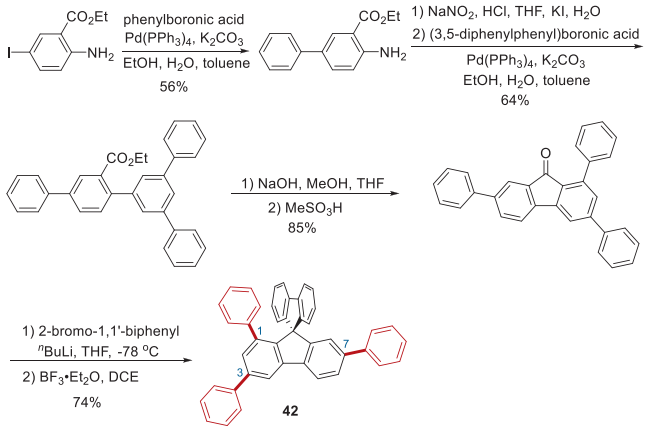
The UV–vis absorption spectra, emission spectra, and quantum yields were measured in [a] toluene or [b] cyclohexane.

PhOLED devices, with **38**, **40**, and **41** serving as the host materials, display EQE_{max} values of 20.2 %, 19.8 %, and 19.9 %, respectively. Host **41** exhibits a higher EQE_{max} of 27.3 % compared to the conventional host material CBP (EQE_{max} = 19.2 %) in red PhOLEDs. It is worth mentioning that the C–H activation strategy offers a new approach for the preparation of high-performance hosts based on C1-substituted SBFs.

In 2024, Lan and Wu *et al.* introduced linear structures into the orthogonal configuration of SBF to enhance carrier mobilities while maintaining high E_T [83]. Initially, the interannular selective C–H arylation of biphenyl-2-formaldehydes was achieved *via* a transient directing group (TDG) strategy under reaction conditions involving $Pd(OAc)_2$ as the catalyst, L–*tert*–leucine as the transient directing group, AgOTFA as the oxidant, and $ZnCO_3$ as the base in TFE at 100 °C in air (Scheme 21). Subsequently, a series of 1,4-diaryl substituted SBFs (**43**–**46**) were synthesized through sequential interannular C–H arylation, intramolecular Friedel-Crafts acylation, nucleophilic addition, and intramolecular Friedel-Crafts alkylation. The T_d of **43**, **44**, **45**,and **46** are 304, 356, 380, and 394 °C, respectively. Additionally, the T_g was measured to be 78 °C for **43**, 97 °C for **44**, and 100 °C for **46** (Table 2). These four 1,4-diaryl SBFs exhibit comparable absorption spectra with peaks at 298 and 310–311 nm, as well as analogous emission spectra peaking at 384–386 nm. Notably, **43**, **44**, and **45**, which possess varying aryl groups at the C1 position, all exhibit identical E_T values of 2.75 eV due to the conjugation-breaking effect between the C1 aryl group and the SBF fragment. All four 1,4-diaryl SBFs demonstrate relatively high carrier mobilities for both holes and electrons. Among them, com-



Scheme 21. Synthesis of multi-substituted SBFs (**43**–**46**) with C1 substitution by interannular C–H arylation of biphenyl-2-formaldehydes. Isolated yield of [a] step I, [b] step II and [c] step III.



Scheme 20. Synthesis of **42**.

pound **44** exhibits the highest mobility and excellent charge balance with u_h of 3.83×10^{-5} cm^2 V^{-1} s^{-1} and u_e of 4.06×10^{-5} cm^2 V^{-1} s^{-1}, attributed to the linearity and relatively good planarity of *para*-quaterphenyl structure. Owing to their sufficiently high E_T, these four 1,4-diaryl SBFs can serve as host materials in RGB PhOLEDs and exhibit excellent device performance (Fig. 10). The PhOLEDs using **44** as host material display EQE_{max} of 26.0%, 26.1%, and 22.5% for red, green, and blue emission, respectively. The coordination of molecular linearity and orthogonality offers novel perspectives for the design and development of universal hosts.

Similarly, the C–H arylation/cyclization reaction of aromatic aldehydes using the TDG strategy also provides an effective route for the synthesis of 1,6- and 1,8-substituted SBFs, which are very rarely reported in the literature and pose significant challenges in terms of synthetic accessibility [76]. Under Pd-catalyzed reaction conditions, 2-bromobenzaldehyde reacted with 3-bromoiodobenzene to afford a mixture of 1,6-diBr-FO and 1,8-diBr-FO (3:1) in 15% yield [84]. Subsequently, the *meta*-terphenyl fragments were introduced *via* Suzuki-Miyaura cross-coupling reaction, yielding 1,6-dimtp-FO and 1,8-dimtp-FO (Scheme 22a). Compounds **47** (1,6-dimtp-SBF) and **48** (1,8-dimtp-SBF) were obtained through nucleophilic addition by (1,1′-biphenyl)-2-yllithium and intramolecular spiroannulation (Schemes 22b and c). The T_d and T_g values of **47** (435 °C, 150 °C) are higher than those of **48** (407 °C, 127 °C). **48** also exhibits a high E_T value of 2.86 eV, which is very close to that of unsubstituted SBF (2.89 eV) owing to the effective disruption of π-conjugation. **47** has a slightly lower E_T value of 2.83 eV. Furthermore, both **47** and **48** demonstrate good charge balance, attributable to their comparable hole and electron mobilities. The device with EML composed of **48** mixed with 2 wt% of DtBuCzB and 10 wt% of FIrpic demonstrates an EQE_{max} as high as 33.9%, and the blue device with EML composed of **48** mixed with 0.5 wt% of *ν*-DABNA and 20 wt% of CN-Ir exhibits an EQE_{max} of 30.9% with an excellent efficiency roll-off value of 21.8% at 1000 cd/m^2, highlighting the potential of multi-substituted SBFs as promising candidates for high-performance blue OLEDs.

The reported multi-substituted SBFs with C1 substituents encompass C1,3, C1,4, C1,6, C1,7, C1,8, and C1,3,7 substitution patterns. Due to the synthetic difficulties, these multi-substituted SBFs are mainly synthesized through the C–H arylative/cyclization strategy. Owing to steric hindrance, a large dihedral angle is formed between the SBF moiety and the C1 substituent, which completely disrupts the π-conjugation. The C1,3-, C1,4-, C1,6-, and C1,8-substituted SBFs have high E_T and wide E_g, while C1,7- and C1,3,7-substituted SBFs exhibit lower E_T and reduced E_g values due to the π-conjugation extension at the C7 position. Notably, multi-substituted SBFs with C1 substituents typically exhibit good charge balance, featuring high and comparable hole and electron mobilities. This may be attributed to intramolecular $\pi \cdots \pi$ interaction between the C1 substituents and the fluorene plane.

5. Multi-substituted SBFs with C4 substitution

Despite the presence of an *ortho*-linked structure in the C4-substituted SBF derivatives, the substantial steric hindrance effect gives rise to a pronounced dihedral angle between the C4 sub-

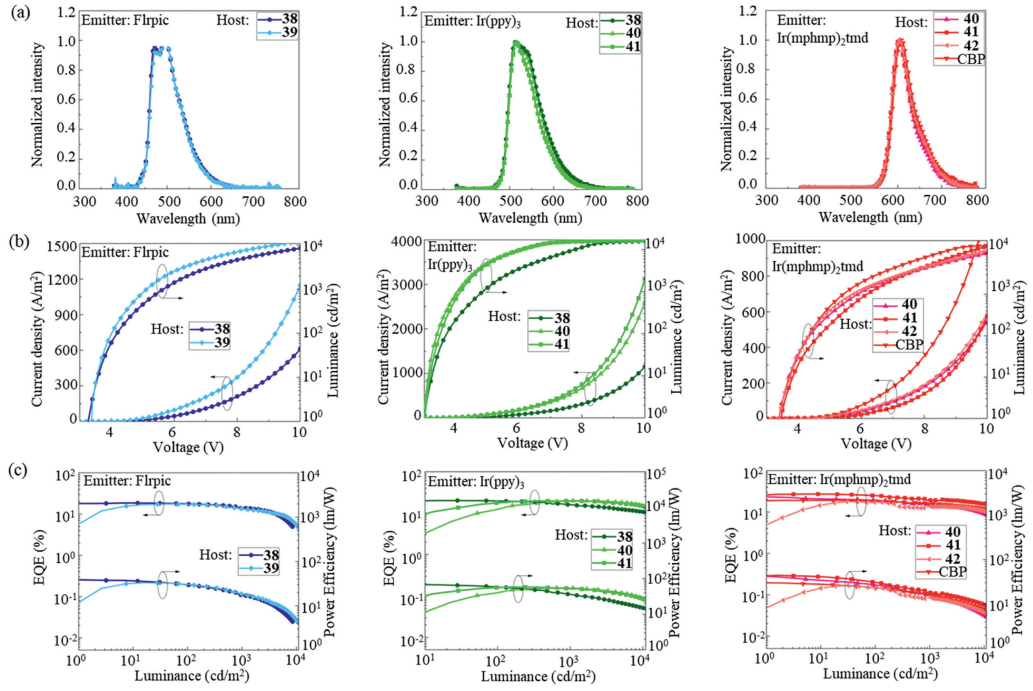


Fig. 9. The performance of PhOLEDs based on **38**–**42**. Reproduced with permission [82]. Copyright 2021, John Wiley & Sons, Inc.

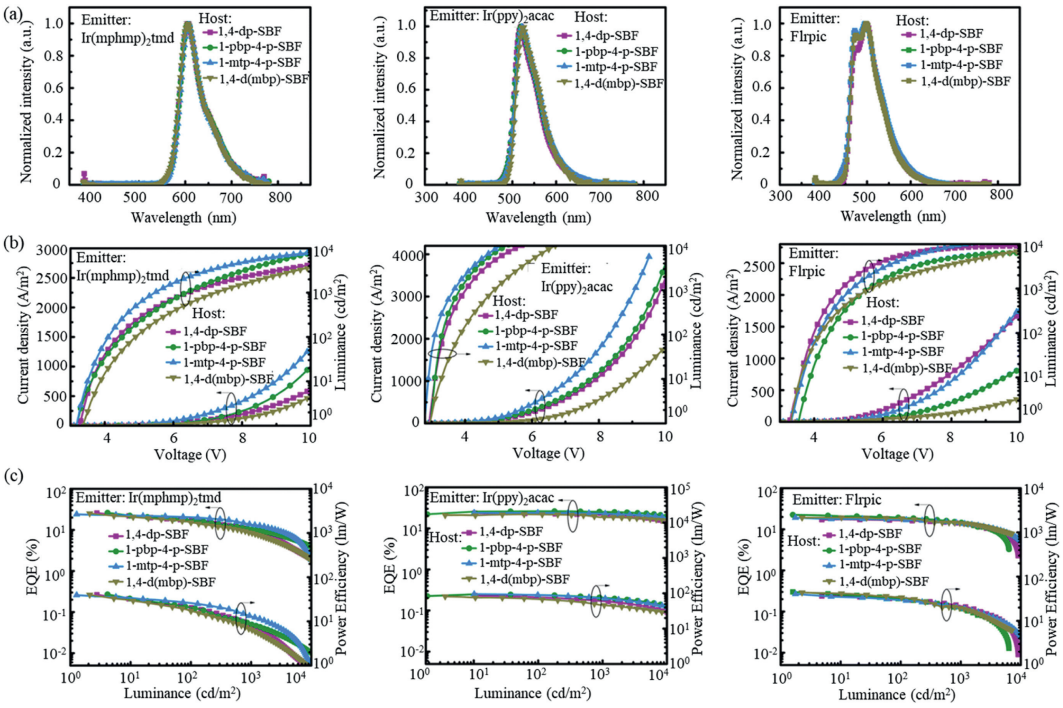
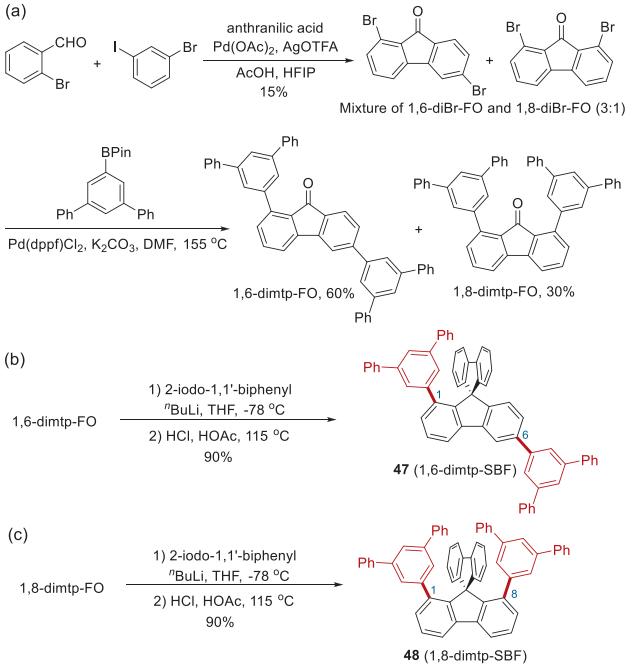
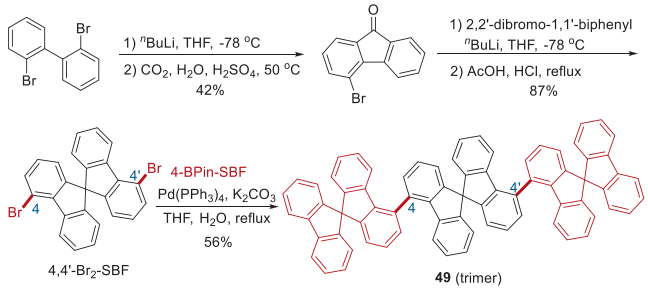


Fig. 10. The performance of PhOLEDs based on **43** (1,4-dp-SBF), **44** (1-pbp-4-p-SBF), **45** (1-mtp-4-p-SBF), and **46** (1,4-d(mbp)-SBF). Reproduced with permission [83]. Copyright 2024, The Royal Society of Chemistry.



Scheme 22. Synthesis of **47** and **48**.



Scheme 23. Synthesis of **49**.

stituent and the fluorene plane, thereby leading to the interruption of conjugation. The size of C4 substituent affects the dihedral angle, thus adjusting the electronic properties. Mono-substituted SBFs with C4 substitution, such as phenyl [85,86], phosphine oxide [87], pyridyl [88], triazine [89], triphenylene [90], and 9,9′-spirobifluorene [44] share a common characteristic of high E_T, which endows them with the potential to serve as universal host materials.

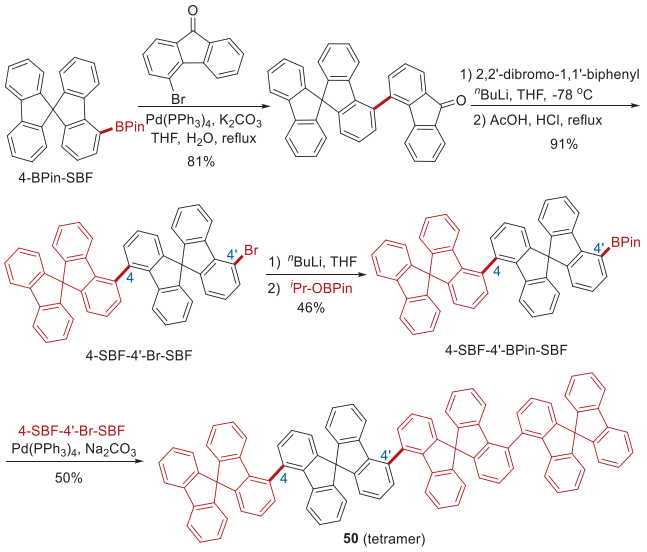
In 2010, Ma and Yang *et al.* synthesized 4,4′-linked tri-, tetra-, and pentamers of SBFs (**49**–**51**) as high E_T PHC hosts [91]. These oligomers were primarily obtained through Suzuki-Miyaura coupling reactions involving 4,4′-halogenated or boronate ester-substituted SBFs (Schemes 23-25), which exhibit excellent morphological stability, with T_g of 244 °C for **49**, 280 °C for **50**, and 326 °C for **51**. **49**, **50**, and **51** show identical absorption (λ_{max} = 308 nm) and emission (λ_{max} = 374 nm) spectra (Table 3). All of these three oligomers display high and identical E_T values of 2.80 eV, attributed to the C4 linkage of SBFs that effectively impedes π-conjugation. The blue and green PhOLEDs utilizing **49** as the host material exhibit EQE_{max} of 11.6% and 17.3%, respectively.

Recently, compound **52** (4,4-dimtp-SBF) was also synthesized with a yield of 76% *via* the Suzuki-Miyaura coupling reaction of the key intermediate 4,4-Br_2-SBF and (3,5-diphenylphenyl)boronic acid (Scheme 26) [76]. Compound **52** demonstrates excellent thermal and morphological stability with a T_d of 463 °C and a T_g of 164 °C (Table 3). **52** displays an absorption spectrum analogous to those of oligomers (**49**–**51**) and a comparable quantum yield (61%), while the maximum emission wavelength is blue-shifted to 361 nm. The E_T of **52** is also maintained at 2.78 eV. The

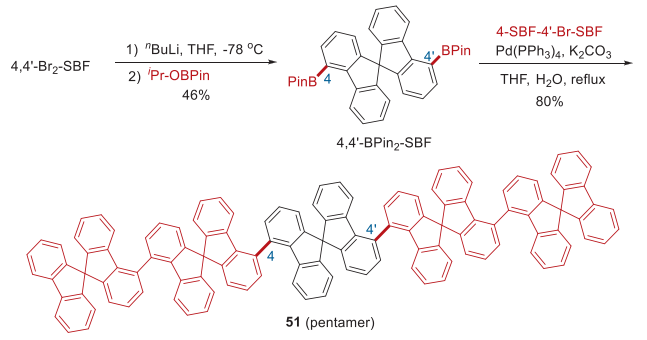
Table 3
Thermal, photophysical, and electrochemical properties of multi-substituted SBFs with C4 substitution (**49**–**52**).

Property	T_d (°C)	T_g (°C)	λ_{abs} (nm)	λ_{em} (nm)	Φ_f (%)	E_T (eV)	HOMO (eV)	LUMO (eV)	E_g (eV)	μ_h ($cm^2\ V^{-1}\ s^{-1}$)	μ_e ($cm^2\ V^{-1}\ s^{-1}$)
49 (trimer) [a]	-	244	308	374	63	2.80	−6.08	−2.15	3.93	-	-
50 (tetramer) [a]	-	280	308	374	58	2.80	−6.08	−2.15	3.93	-	-
51 (pentamer) [a]	-	326	308	374	60	2.80	−6.08	−2.15	3.93	-	-
52 (4,4-dimtp-SBF) [b]	463	164	308	361	61	2.78	−6.01	−2.12	3.89	7.58×10^{-6}	6.81×10^{-6}

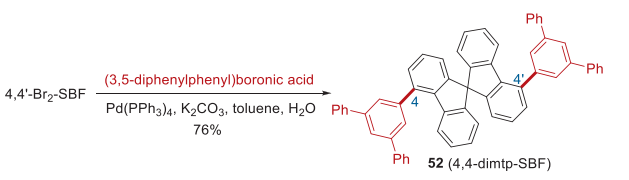
The UV–vis absorption spectra, emission spectra, and quantum yields were measured in toluene [a] or cyclohexane [b].



Scheme 24. Synthesis of **50**.



Scheme 25. Synthesis of **51**.



Scheme 26. Synthesis of **52**.

phosphorescence-sensitized MR-TADF OLEDs display very high performance with EQE_{max} above 30 %, when using **52** as the host material, along with different phosphorescent sensitizers (FIrpic, *fac*-Ir(tpz)$_3$, CN-Ir) and emitters (DtBuCzB and *ν*-DABNA).

All these C4,4′-disubstituted SBFs possess high thermal and morphological stability. The introduction of aryl groups slightly reduces the E_T, but this does not significantly affect their application potential as universal host materials.

6. Conclusion

In summary, the strategic introduction of substituents at specific sites on the SBF framework provides an effective approach to access multi-substituted SBF derivatives. This design strategy enables precise fine-tuning of the electronic and physical properties of target materials, thereby laying a solid foundation for the development of high-performance OLED devices. Multi-substituted SBFs are typically synthesized using multi-halogenated or multi-boronate ester-substituted SBF derivatives as precursors. In addition, transition metal-catalyzed C–H arylation has also been a highly effective and versatile method for constructing structurally complex multi-substituted SBFs. Multi-substituted SBFs generally exhibit remarkable thermal and morphological stability, characterized by high T_d and T_g, which effectively reduce the risk of phase separation during the OLED fabrication process. The photophysical and electrochemical properties of SBFs can be precisely modulated by integrating multiple substituents, thereby providing more opportunities for the optimization of device performances. The incorporation of electron-donating or electron-withdrawing substituents endows the resulting SBFs with the potential to serve as hole-transport or electron-transport materials in OLEDs. The triplet energies (E_T) of multi-substituted SBFs with C2 substitution are generally low due to the complete π-conjugation extension between the C2 substituent and the fluorene plane. Conversely, multi-substituted SBFs with C1, C3, or C4 substitution exhibit relatively high E_T, making them promising universal host materials for RGB PhOLEDs. Multi-substituted SBFs demonstrate superior device performance when utilized as emitters, hosts, electron-transport materials, or hole-transport materials in OLED devices.

Although OLED technology has achieved promising advancements, its further development still demands addressing key challenges, such as improving electroluminescence efficiency, extending device lifetime, and mitigating efficiency roll-off, especially for blue OLEDs. Furthermore, advancing solution-processing techniques is critical to enable large-scale manufacturing and low-temperature fabrication. Additionally, exploring devices with simplified architecture can further reduce the manufacturing costs of OLED devices. Concurrently, the development of alternatives to expensive rare metal complex-based phosphorescent materials is also advancing, which will help reduce material costs and further improve device performance. With sustained research efforts and technological innovations, these challenges will be effectively tackled, thereby paving the way for the advent of next-generation OLED technologies.

Declaration of competing interest

The authors declare that they have no known competing financial interests or personal relationships that could have appeared to influence the work reported in this paper.

CRediT authorship contribution statement

Zhanhui He: Writing – original draft. **Zheng Liu:** Writing – review & editing, Writing – original draft. **Hongji Li:** Writing – origi-

nal draft. **Lijun Yang:** Writing – original draft. **Guodong Yin:** Writing – original draft. **Jingbo Lan:** Writing – review & editing.

Acknowledgments

This work was supported by the National Natural Science Foundation of China (Nos. 22301071, 22571212, and 22371196), the Special Fund Project for Guiding Local Science and Technology Development of Hubei Province by the Central Government (No. 2024CSA097), Excellent Young and Middle-aged Science and Technology Innovation Team Program of Universities in Hubei Province (No. T2024014), Natural Science Foundation of Hubei Province (No. 2023AFB459), and the Hubei Key Laboratory of Pollutant Analysis & Reuse Technology (No. PA220204).

References

[1] T.P.I. Saragi, T. Spehr, A. Siebert, T. Fuhrmann-Lieker, J. Salbeck, Chem. Rev. 107 (2007) 1011–1065.
[2] S. Liu, D. Xia, M. Baumgarten, ChemPlusChem 86 (2021) 36–48.
[3] M. Sun, R. Xu, L. Xie, Y. Wei, W. Huang, Chin. J. Chem. 33 (2015) 815–827.
[4] C. Poriel, J. Rault-Berthelot, Chem. Soc. Rev. 52 (2023) 6754–6805.
[5] C. Poriel, J. Rault-Berthelot, Adv. Funct. Mater. 30 (2020) 1910040.
[6] J. Urieta-Mora, I. García-Benito, A. Molina-Ontoria, N. Martín, Chem. Soc. Rev. 47 (2018) 8541–8571.
[7] H.W. Luo, Z.T. Liu, Chin. Chem. Lett. 27 (2016) 1283–1292.
[8] F. Ullah, H. Chen, C.Z. Li, Chin. Chem. Lett. 28 (2017) 503–511.
[9] X. Sun, D. Zhao, Z.A. Li, Chin. Chem. Lett. 29 (2018) 219–231.
[10] Y. Guo, G. Yu, Y. Liu, Adv. Mater. 22 (2010) 4427–4447.
[11] Y. Yan, C. Zhao, J. Hui, et al., Chin. Chem. Lett. 37 (2026) 111343.
[12] Y. Jiang, Y.Y. Liu, X. Liu, et al., Chem. Soc. Rev. 49 (2020) 5885–5944.
[13] M. Shimizu, T. Sakurai, Aggregate 3 (2022) e144.
[14] Y. Tao, C. Yang, J. Qin, Chem. Soc. Rev. 40 (2011) 2943–2970.
[15] A. Chaskar, H.F. Chen, K.T. Wong, Adv. Mater. 23 (2011) 3876–3895.
[16] J.A. Kang, J. Lim, J.Y. Lee, Mater. Chem. Front. 6 (2022) 757–764.
[17] S.S.S. Shahnawaz, M.R. Nagar, J. Mater. Chem. C 7 (2019) 7144–7158.
[18] X. Yang, G. Zhou, W.Y. Wong, Chem. Soc. Rev. 44 (2015) 8484–8575.
[19] Y. Xu, P. Xu, D. Hu, Y. Ma, Chem. Soc. Rev. 50 (2021) 1030–1069.
[20] C. Giebeler, H. Antoniadis, D.D.C. Bradley, Y. Shirota, J. Appl. Phys. 85 (1999) 608–615.
[21] D. Zhang, L. Duan, J. Phys. Chem. Lett. 10 (2019) 2528–2537.
[22] S. Jhulki, J.N. Moorthy, J. Mater. Chem. C 6 (2018) 8280–8325.
[23] M. Shimizu, T. Hiyama, Chem. Asian J. 5 (2010) 1516–1531.
[24] L. Zhao, C. Duan, D. Ding, et al., Chin. Chem. Lett. 32 (2021) 397–400.
[25] R. Pudzich, T. Fuhrmann-Lieker, J. Salbeck, Adv. Polym. Sci. 199 (2006) 83–142.
[26] C. Poriel, J. Rault-Berthelot, Adv. Funct. Mater. 31 (2021) 2010547.
[27] Y. Chen, J. Xu, P. Gao, Org. Chem. Front. 11 (2024) 508–539.
[28] R.G. Clarkson, M. Gomberg, J. Am. Chem. Soc. 52 (1930) 2881–2891.
[29] J.C. Hood, D.A. Klumpp, J. Org. Chem. 88 (2023) 665–669.
[30] L. Sicard, C. Quinton, J.D. Peltier, et al., Chem. Eur. J. 23 (2017) 7719–7727.
[31] C. Poriel, J. Rault-Berthelot, J. Mater. Chem. C 5 (2017) 3869–3897.
[32] C. Poriel, L. Sicard, J. Rault-Berthelot, Chem. Commun. 55 (2019) 14238–14254.
[33] S. Thiery, C. Declairieux, D. Tondelier, et al., Tetrahedron 70 (2014) 6337–6351.
[34] J.F. Liu, X.Q. Wang, Y.J. Yu, et al., Org. Electron. 91 (2021) 106088.
[35] J. Tang, Y. Chen, L. Cong, B. Lin, Y. Sun, Tetrahedron 70 (2014) 3847–3853.
[36] S.C. Dong, C.H. Gao, X.D. Yuan, et al., Org. Electron. 14 (2013) 902–908.
[37] S.C. Dong, C.H. Gao, Z.H. Zhang, et al., Phys. Chem. Chem. Phys. 14 (2012) 14224–14228.
[38] C. Poriel, C. Quinton, F. Lucas, et al., Adv. Funct. Mater. 31 (2021) 2104980.
[39] D.M.E. Freeman, A.J. Musser, J.M. Frost, et al., J. Am. Chem. Soc. 139 (2017) 11073–11080.
[40] Y. Wang, W. Liu, J. Deng, et al., Chem. Asian J. 11 (2016) 2555–2563.
[41] C. Poriel, Y. Ferrand, S. Juillard, P. Le Maux, G. Simonneaux, Tetrahedron 60 (2004) 145–158.
[42] Y. Jiang, K.F. Li, K. Gao, et al., Angew. Chem. Int. Ed. 60 (2021) 10007–10015.
[43] Y.J. Yu, Z.H. Qu, L.Y. Ding, et al., Adv. Funct. Mater. 34 (2024) 2405491.
[44] Z. Jiang, H. Yao, Z. Zhang, et al., Org. Lett. 11 (2009) 2607–2610.
[45] S. Tao, Z. Peng, X. Zhang, et al., Adv. Funct. Mater. 15 (2005) 1716–1721.
[46] X.Y. Cao, W. Zhang, H. Zi, J. Pei, Org. Lett. 6 (2004) 4845–4848.
[47] C. Poriel, J. Rault-Berthelot, Acc. Mater. Res. 3 (2022) 379–390.
[48] C. Poriel, J. Rault-Berthelot, Z.Q. Jiang, Mater. Chem. Front. 6 (2022) 1246–1252.
[49] Y. Yuan, Y. Hu, Y.X. Zhang, et al., Adv. Funct. Mater. 27 (2017) 1700986.
[50] Y.J. Yu, Y. Hu, S.Y. Yang, et al., Angew. Chem. Int. Ed. 59 (2020) 21578–21584.
[51] X. Ren, J. Li, R.J. Holmes, et al., Chem. Mater. 16 (2004) 4743–4747.
[52] K.T. Wong, Y.Y. Chien, R.T. Chen, et al., J. Am. Chem. Soc. 124 (2002) 11576–11577.
[53] C.C. Wu, Y.T. Lin, H.H. Chiang, et al., Appl. Phys. Lett. 81 (2002) 577–579.
[54] A.P. Kulkarni, C.J. Tonzola, A. Babel, S.A. Jenekhe, Chem. Mater. 16 (2004) 4556–4573.
[55] O. Usluer, S. Demic, D.A.M. Egbe, et al., Adv. Funct. Mater. 20 (2010) 4152–4161.
[56] N. Nagamura, H. Sasabe, H. Sato, et al., Chem. Eur. J. 29 (2023) e202202636.
[57] J. Pei, J. Ni, X.H. Zhou, X.Y. Cao, Y.H. Lai, J. Org. Chem. 67 (2002) 4924–4936.
[58] C. Poriel, J. Rault-Berthelot, Acc. Mater. Res. 4 (2023) 733–745.
[59] S. Thiery, D. Tondelier, B. Geffroy, et al., Org. Lett. 17 (2015) 4682–4685.
[60] W.J. Shen, R. Dodda, C.C. Wu, et al., Chem. Mater. 16 (2004) 930–934.
[61] K.T. Wong, Y.L. Liao, Y.T. Lin, H.C. Su, C.C. Wu, Org. Lett. 7 (2005) 5131–5134.
[62] K.T. Wong, Y.L. Liao, Y.C. Peng, et al., Cryst. Growth Des. 5 (2005) 667–671.
[63] M.Y. Lai, C.H. Chen, W.S. Huang, et al., Angew. Chem. Int. Ed. 47 (2008) 581–585.
[64] C.H. Chen, W.S. Huang, M.Y. Lai, et al., Adv. Funct. Mater. 19 (2009) 2661–2670.
[65] W.Y. Hung, T.C. Tsai, S.Y. Ku, L.C. Chi, K.T. Wong, Phys. Chem. Chem. Phys. 10 (2008) 5822–5825.
[66] Y.Y. Chien, K.T. Wong, P.T. Chou, Y.M. Cheng, Chem. Commun. (2002) 2874–2875.
[67] Y. Zheng, Z. Wang, Z. Zhong, et al., Dyes Pigm. 194 (2021) 109550.
[68] S. Thiery, B. Heinrich, B. Donnio, C. Poriel, F. Camerel, J. Phys. Chem. C 119 (2015) 10564–10575.
[69] L.S. Cui, S.C. Dong, Y. Liu, et al., Org. Electron. 14 (2013) 1924–1930.
[70] L. Ding, S. Du, L.S. Cui, F.H. Zhang, L.S. Liao, Org. Electron. 37 (2016) 108–114.
[71] L.S. Cui, Y.M. Xie, Y.K. Wang, et al., Adv. Mater. 27 (2015) 4213–4217.
[72] N. Fomina, T.E. Hogen-Esch, Macromolecules 41 (2008) 3765–3768.
[73] D. Ari, Y.J. Yang, C. Quinton, et al., Angew. Chem. Int. Ed. 63 (2024) e202403066.
[74] Q. Wang, F. Lucas, C. Quinton, et al., Chem. Sci. 11 (2020) 4887–4894.
[75] Q. Li, Y. Guo, J. Lan, et al., Chem. Sci. 15 (2024) 16096–16102.
[76] Y.J. Yang, D. Ari, Z.H. Yu, et al., Angew. Chem. Int. Ed. 64 (2025) e202501895.
[77] N.A. van Dantzig, D.H. Levy, C. Vigo, P. Piotrowiak, J. Chem. Phys. 103 (1995) 4894–4906.
[78] L. Sicard, C. Quinton, F. Lucas, et al., J. Phys. Chem. C 123 (2019) 19094–19104.
[79] F.C. Kong, Y.L. Zhang, C. Quinton, et al., Angew. Chem. Int. Ed. 61 (2022) e202207204.
[80] L. Sicard, C. Brouillac, N. Leclerc, et al., Mater. Chem. Front. 8 (2024) 1349–1361.
[81] L.J. Sicard, H.C. Li, Q. Wang, et al., Angew. Chem. Int. Ed. 58 (2019) 3848–3853.
[82] Y. Luo, Z. Liu, G. Yang, et al., Angew. Chem. Int. Ed. 60 (2021) 18852–18859.
[83] Q. Li, Z. Yu, Q. Liu, et al., Chem. Sci. 15 (2024) 10547–10555.
[84] X.Y. Chen, S. Ozturk, E.J. Sorensen, Org. Lett. 19 (2017) 1140–1143.
[85] S. Thiery, D. Tondelier, C. Declairieux, et al., J. Mater. Chem. C 2 (2014) 4156–4166.
[86] C. Quinton, S. Thiery, O. Jeannin, et al., ACS. Appl. Mater. Interfaces 9 (2017) 6194–6206.
[87] S.E. Jang, C.W. Joo, S.O. Jeon, K.S. Yook, J.Y. Lee, Org. Electron. 11 (2010) 1059–1065.
[88] S. Thiery, D. Tondelier, C. Declairieux, et al., J. Phys. Chem. C 119 (2015) 5790–5805.
[89] J. Ha, S.C. Kim, M. Jung, J.Y. Lee, J. Mater. Chem. C 10 (2022) 5962–5969.
[90] X. Tang, Y. Li, Y.K. Qu, et al., Adv. Funct. Mater. 30 (2020) 1910633.
[91] C. Fan, Y. Chen, P. Gan, et al., Org. Lett. 12 (2010) 5648–5651.